Sonic horizons and causality in phase transition dynamics

Debasis Sadhukhan [1], Aritra Sinha [1], Anna Francuz,[1] Justyna Stefaniak [1], Marek M. Rams [1], Jacek Dziarmaga,[1]
and Wojciech H. Zurek[2]

[1]*Institute of Theoretical Physics, Jagiellonian University, Łojasiewicza 11, 30-348 Kraków, Poland*
[2]*Theory Division, Los Alamos National Laboratory, Los Alamos, New Mexico 87545, USA*

A system gradually driven through a symmetry-breaking phase transition is subject to the Kibble-Zurek mechanism (KZM). As a consequence of the critical slowing down, its state cannot follow local equilibrium, and its evolution becomes nonadiabatic near the critical point. In the simplest approximation, that stage can be regarded as an "impulse" where the state of the system remains unchanged. It leads to the correct KZM scaling laws. However, such a "freeze-out" might suggest that the coherence length of the nascent order parameter remains unchanged as the critical region is traversed. By contrast, the original causality-based discussion emphasized the role of the *sonic horizon*: Domains of the broken symmetry phase can expand with a velocity limited by the speed of the relevant sound. This effect was demonstrated in the quantum Ising chain where the dynamical exponent $z = 1$ and quasiparticles excited by the transition have a fixed speed of sound. To elucidate the role of the sonic horizon, in this paper we study two systems with $z > 1$ where the speed of sound is no longer fixed, and the fastest excited quasiparticles set the size of the sonic horizon. Their effective speed decays with increasing transition time. In the extreme case, the dynamical exponent z can diverge such as in the Griffiths region of the random Ising chain where the localization of excited quasiparticles freezes the growth of the correlation range when the critical region is traversed. Of particular interest is an example with $z < 1$, the long-range extended Ising chain, where there is no upper limit to the velocity of excited quasiparticles with small momenta. Initially, the power-law tail of the correlation function grows adiabatically, but in the nonadiabatic stage it lags behind the adiabatic evolution.

I. INTRODUCTION

The Kibble-Zurek mechanism (KZM) evolved from the scenario for defect creation in cosmological symmetry-breaking phase transitions [1]. As the post-Big-Bang Universe cools, causally disconnected regions must choose a broken symmetry vacuum independently. Such random choices lead to topologically nontrivial configurations that survive phase ordering as topological defects. In the cosmological setting the average size of the causally connected regions (hence, the average density of defects) is set by the Hubble radius at the time of the transition. This early Universe scenario relies on the speed of light and does not apply to the laboratory phase transitions. However, it was the point of departure for the dynamical theory [2,3] that employs critical exponents of the transition and the quench time to predict the scaling of the resulting density of defects. KZM was successfully tested using numerical simulations [4–16] and laboratory experiments in condensed matter systems [17–40]. More recently, KZM was adapted to quantum phase transitions [41–46]. Theoretical developments [47–66] and experimental tests [67–75] of quantum KZM (QKZM) followed. The recent experiment [75], where a quantum Ising chain in the transverse field is emulated using Rydberg atoms, is fully consistent with the predicted scaling [43,44].

The KZM is often presented in its cartoon version where, due to the critical slowing down/closing of the energy gap, the dynamics of the system literally freezes out in the neighborhood of the critical point. Today, as the experiments are able not only to count the final number of defects but can also monitor and probe the state of the system during the transition, it is timely to reinvestigate the causally limited spreading of correlations during the putative "freeze-out" stage of the evolution.

In QKZM a system initially prepared in its ground state is smoothly ramped across a critical point to the other side of the quantum phase transition. A distance from the critical point, measured by a dimensionless parameter ϵ controlling a Hamiltonian, can be linearized close to the critical point as

$$\epsilon(t) = \frac{t}{\tau_Q}. \tag{1}$$

Here, τ_Q is a quench time. Initially, far from the critical point, the evolution is adiabatic, and the system follows its adiabatic ground state (see Fig. 1). The adiabaticity fails at $-\hat{t}$ when the reaction time of the system given by the inverse of the gap becomes slower than the timescale $|\epsilon/\dot{\epsilon}| = |t|$ on which the transition is being imposed. The gap closes as $\Delta \simeq |\epsilon|^{z\nu}$, where z and ν are the dynamical and correlation length exponents, respectively. From the equation $|t| \simeq |t/\tau_Q|^{-z\nu}$ we obtain $\hat{t} \simeq \tau_Q^{z\nu/(1+z\nu)}$ and the corresponding $\hat{\epsilon} = \hat{t}/\tau_Q \simeq \tau_Q^{1/(1+z\nu)}$. In the naive "freeze-out" version of the impulse approximation the ground state at $-\hat{\epsilon}$, with a corresponding
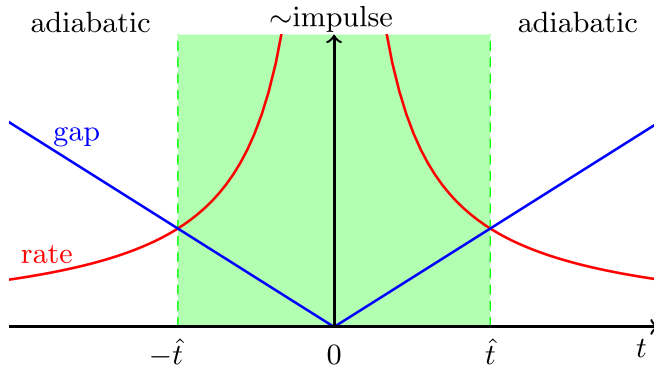
FIG. 1. Adiabatic-impulse-adiabatic view of KZM. A linear ramp crosses the critical point at time $t = 0$. The instantaneous transition rate $|\dot{\epsilon}/\epsilon| = 1/|t|$ diverges at the critical point and the relevant energy gap closes as $|\epsilon|^{z\nu}$. Consequently, while before $-\hat{t}$ the state follows the adiabatic ground state, near the critical point (between $-\hat{t}$ and $\hat{t}$) its evolution is nonadiabatic. The freeze-out assumes that the state is "frozen" at $-\hat{t}$—the size of the domains of the nascent phase does not change until $+\hat{t}$, where the state starts to "catch up" with the Hamiltonian. This version of KZM ignores propagation of the new phase front in the time interval $(-\hat{t}, +\hat{t})$. It yields correct scalings, but it does not capture what happens, for example, in the paramagnetic-ferromagnetic quantum phase transition in the quantum Ising chain in a transverse field [76,77]. Nevertheless, it may well be relevant in phase transitions where the conserved order parameter or other causes (localization) impede the propagation of phase fronts of the broken symmetry phase.

correlation length

$$\hat{\xi} \simeq \tau_Q^{\nu/(1+z\nu)}, \tag{2}$$

is expected to characterize the state of the system until $+\hat{t}$, when the evolution can restart. In this way, $\hat{\xi}$ becomes imprinted on the initial state for the final adiabatic stage of the evolution after $+\hat{t}$. Simplistic as it is, the adiabatic-impulse-adiabatic approximation correctly predicts the scaling of the characteristic length scale $\hat{\xi}$ and the timescale

$$\hat{t} \simeq \hat{\xi}^z, \tag{3}$$

with the critical exponents and τ_Q. They both diverge in the adiabatic limit $\tau_Q \to \infty$, where they become the unique relevant scales in the KZ scaling ansatz [76–78]. For instance, a two-point correlation function $C_R(t)$, between two sites separated by a distance R, should satisfy

$$\hat{\xi}^\Delta C_R(t) = F(t/\hat{\xi}^z, R/\hat{\xi}). \tag{4}$$

Here, Δ is a scaling dimension and F a nonuniversal scaling function. Equation (4) is expected to be accurate in the long-wavelength and low-frequency limit. It is worth observing here that the crude adiabatic-impulse-adiabatic approximation is consistent with the scaling hypothesis (4). However, it implies a particular (time-independent) form of the scaling function F.

As emphasized already in the early papers (see Refs. [2,3]), the freeze-out is not the complete story, and often not even a good approximation. A simple "sonic horizon" argument
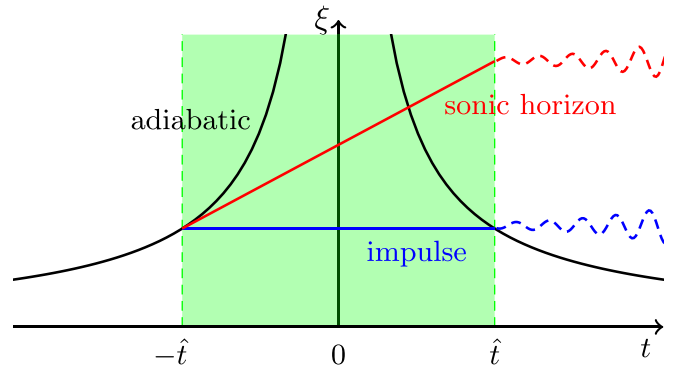

FIG. 2. Sonic horizon view of KZM. Initially, the correlation length ξ follows adiabatically the equilibrium healing length that, in the adiabatic ground state (black), diverges at the critical point. Critical slowing down means that the size of the correlation length will begin to lag behind the values dictated by the ground state of the Hamiltonian at about $-\hat{t}$. Pretransition fluctuations reach size $\hat{\xi}$ at that instant and seed the subsequent evolution of the system. The new broken symmetry phase is therefore selected by fluctuations in domains if size $\hat{\xi}$ at $-\hat{t}$. Broken symmetry spreads within the impulse time interval of $2\hat{t}$ with the velocity $2\hat{v}$ in every direction, enlarging the resulting "sound cone" to roughly $5\hat{\xi}$ by $\hat{t}$. In the freeze-out approximation (blue), after $-\hat{t}$ the correlation length freezes, and remains close to the adiabatic correlation length at $-\hat{t}$. Both the freeze-out and the sonic horizon views lead to the same scalings, but they result in different estimates of the prefactors for domain sizes and defect densities.

appealing to causality that goes beyond the impulse approximation is often more accurate. It is illustrated schematically in Fig. 2. As long as the evolution is adiabatic, the rate of growth of the diverging adiabatic correlation length $\xi \simeq |\epsilon|^{-\nu}$ is

$$\frac{d\xi}{dt} = \frac{d\epsilon}{dt}\frac{d\xi}{d\epsilon} = \frac{1}{\tau_Q}\frac{\nu}{|\epsilon|^{\nu+1}}. \tag{5}$$

This rate diverges at the critical point. Hence there must be time $-\hat{t}$ when it exceeds the speed limit set by twice

$$\hat{v} \simeq \frac{\hat{\xi}}{\hat{t}} \simeq \tau_Q^{-\nu(z-1)/(1+z\nu)}. \tag{6}$$

The scaling of $-\hat{t}$ obtained in this way is the same as in Eq. (3).

Causality and the KZ velocity $\hat{v}$ are also central for the shortcuts to adiabaticity via inhomogeneous KZM. Therein, the external driving field has a smooth position dependence, gradually taking the system across the critical point, one part after another. The velocity of the driven critical front below $\hat{v}$ (which in general depends on the shape of the above position dependence) is expected to pave the way to adiabatic dynamics, both for classical [6,79–83] and for quantum [84–89] systems.

In the QKZM the speed limit is central to the causal argument. It originates from the dispersion of quasiparticles at the critical point $\omega \simeq k^z$. Their speed for a quasimomentum k is $v = d\omega/dk \simeq k^{z-1}$. Between $-\hat{t}$ and $\hat{t}$ the quench excites quasiparticles with a magnitude of k up to $\hat{k} \simeq \hat{\xi}^{-1}$. The speed of quasiparticles with the largest excited k is therefore

$\hat{v} \simeq \hat{k}^{z-1} \simeq \hat{\xi}^{1-z} \simeq \hat{\xi}/\hat{t}$. When $z \geqslant 1$, $\hat{v}$ is an upper bound on the velocity of quasiparticles. A quench in a translationally invariant system excites entangled pairs of quasiparticles with opposite quasimomenta, k and $-k$. When moving apart, they are spreading correlations across the system. For $z \geqslant 1$ the rate of correlation spreading is limited by twice the speed $\hat{v}$ of the fastest quasiparticles.

In the crudest version, neglecting in particular the dependence of $\hat{v}$ on the distance from the critical point, the argument implies that after $-\hat{t}$ the correlation range (i.e., the "sonic cone") continues to grow at a rate $2\hat{v}$ until $+\hat{t}$. By this time, the range increases from the initial $\hat{\xi}$ at $-\hat{t}$ to a final $\hat{\xi} + 2\hat{v} \times 2\hat{t} \approx 5\hat{\xi}$. The growth is roughly fivefold. Even if the 5 is just a very rough estimate, it shows how much the actual evolution can differ from the impulse approximation. Nevertheless, this argument confirms the role of $\hat{\xi}$ as the key relevant scale of length. With or without the prefactor of 5, the final correlation length is proportional to $\hat{\xi}$, i.e., it scales with τ_Q in the same way as given by Eq. (2).

From another perspective, in the impulse approximation, the adiabatic ground state $|\psi\rangle$ corresponding to $-\hat{t}$ freezes out as the state of the system. After $-\hat{t}$ the adiabatic ground state departs from the frozen state. The frozen state becomes a superposition over the adiabatic eigenbasis $|n\rangle$, $\sum_n c_n(t)|n\rangle$, where $c_n(t) = \langle n|\psi\rangle$. As a first step beyond the impulse approximation, we can include approximate dynamical phases, $\sum_n c_n(t)e^{-i\omega_n t}|n\rangle$, where ω_n is the adiabatic eigenfrequency at the critical point. In a (noninteracting) translationally invariant system, the eigenstates consist of pairs of excited quasiparticles $|k, -k\rangle$ and the eigenfrequencies are sums of $2\omega_k$. The dynamical phase factors become scrambled—and the phases begin to appear random—when the largest of them, $2\omega_{\hat{k}}t \propto \hat{k}^z t$, becomes comparable to 1 near $\hat{t}$. The dephasing begins when the evolution crosses over from the nonadiabatic KZ stage to the post-KZ adiabatic stage. That is when the phases definitely can no longer be ignored, but even before the crossover the phase factors $e^{-2i\omega_k t}$ make the quasiparticle phase fronts propagate and let the quasiparticles spread the correlations across the system.

For $z = 1$, when the dispersion is linear in k, the quasiparticles have a definite speed of sound. This effect was termed the quasiparticle event horizon [90]. In the QKZM context, it was considered in Refs. [76,77]—see Fig. 3 for an example of the prototypical one-dimensional (1D) quantum Ising model.

In this paper we go beyond $z = 1$ and present two examples with $z > 1$: the classical Ising model with Glauber dynamics in Sec. II and the generalized quantum XY chain in Sec. III. They both exhibit an effective event horizon with a speed limit that depends on the quench time τ_Q. The generic scenario is delimited by two examples where the sonic horizon effect ceases to manifest because one of its underlying assumptions is not satisfied. The first one is the random Ising model in Sec. IV, where localization of excited quasiparticles prevents the spreading of correlations, thus yielding in effect a "freeze-out." The other is the extended Ising model with long-range interactions in Sec. V, where the dynamical exponent z is less than 1. The excited quasiparticles with $k \to 0$ have infinite velocity, and the speed $\hat{v}$ at the maximal excited $\hat{k}$ is not an upper but a lower speed limit. Consequently, there is no sonic horizon effect, and the correlations have a long-range
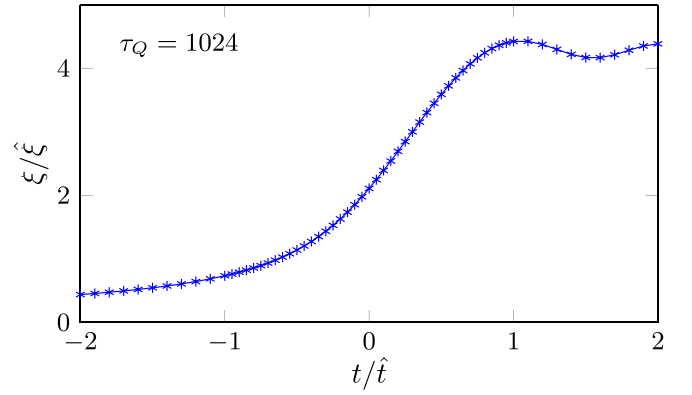

FIG. 3. Quantum Ising chain. The correlation length during the quench in the 1D quantum Ising model, $H = -\sum_n (1 - \epsilon)\sigma_n^z + \sigma_n^x \sigma_{n+1}^x$, where the dynamical critical exponent $z = 1$ and the excited quasiparticles possess a definite speed of sound. Compare with Fig. 2. Data from Ref. [77].

power-law tail that can evolve in time. After $-\hat{t}$ the tail begins to lag behind its adiabatic evolution. However, instead of completely freezing out, it continues to grow at a finite rate.

II. CLASSICAL ISING MODEL: $z = 2$

We begin with the classic example of the classical Ising model on a periodic square lattice of size $L \times L$,

$$H = -\sum_{\langle j, j'\rangle} \sigma_j^z \sigma_{j'}^z. \tag{7}$$

On an infinite lattice, the critical inverse temperature would be $\beta_c = \ln(1 + \sqrt{2})/2 \simeq 0.4407$. The relevant equilibrium exponents are $\nu = 1$ and $\eta = 1/4$ [91]. We model relaxation to an external heat bath with the Glauber dynamics: A Monte Carlo update thermalizes one spin (chosen at random) at a time. The time needed for L^2 such one-spin updates sets the unit of time. For such a simple relaxation, the dynamical exponent is $z = 2$, belonging to the universality class of model-A dynamics [92]. We performed all our numerical simulations on a 4096×4096 lattice. This lattice size is 100 times longer than the longest correlation range encountered in the simulations, hence any finite-size effects are eliminated with a wide safety margin. All results were averaged over 50 repetitions of the quench, each of them starting from a different initial random spin configuration at infinite temperature.

The inverse temperature of the heat bath is ramped linearly in time,

$$\beta(t) = \beta_c\left(1 + \frac{t}{\tau_Q}\right), \tag{8}$$

starting with a random spin configuration at $\beta(-\tau_Q) = 0$. Figure 4(a) shows the energy E during the ramp as a function of β for different quench times τ_Q. Generally, the system is more ordered for slower quenches. For slow enough quenches, the KZ picture emerges. The system evolves adiabatically until it begins to go out of equilibrium around $-\hat{t}$, where $\hat{t} \simeq \tau_Q^{2/3}$ is the KZ timescale.

In order to see how the excitation energy should depend on the quench time, let us consider the equilibrium internal
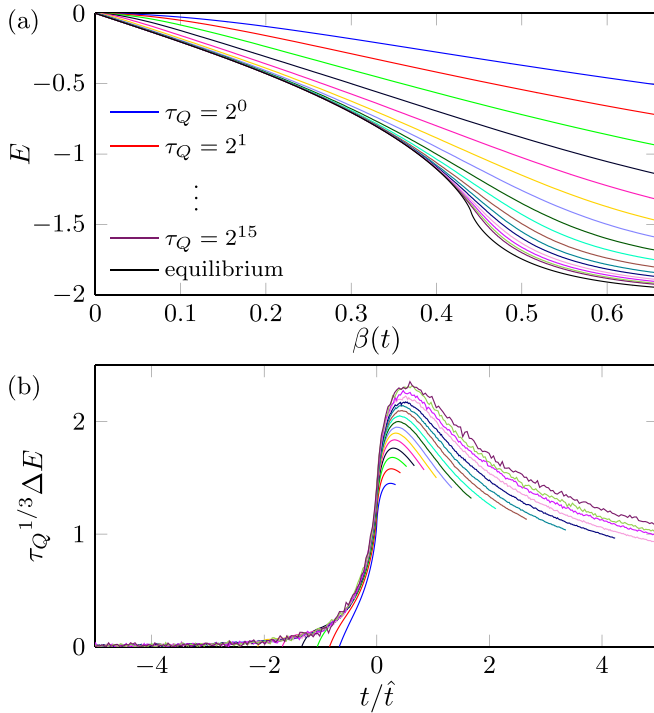
FIG. 4. Classical Ising model in 2D on a square lattice. In (a), energy per site E as a function of $\beta(t)$ for different quench times τ_Q. For reference, the black line is the equilibrium internal energy $U(\beta)$. With increasing quench time, the quench curves converge to the equilibrium one. In (b), excitation energy per site, $\Delta E = E - U$, as a function of scaled time for different quench times τ_Q. Here, both ΔE and t are rescaled according to the KZM predictions. For large $\tau_Q \gg 1$ the scaling makes them collapse in the KZ regime between $t \approx -\hat{t}$ and $t \approx \hat{t}$, corresponding to the rescaled times -1 and $+1$, respectively. At later times the phase ordering kinetics steps in, which goes beyond the KZ physics.

energy. Near the critical point it is

$$U(\beta) = -[1 + A(\beta - \beta_c)\ln|\beta - \beta_c|]/\tanh\beta_c, \quad (9)$$

where $A \simeq 1$ is a constant. In the adiabatic-impulse approximation the state becomes effectively frozen near $-\hat{t}$ when $\beta_c - \hat{\beta} \simeq \tau_Q^{-1/3}$. At β_c the energies of the frozen state (i.e., the instantaneous state at $-\hat{t}$) and the equilibrium one differ by

$$\begin{aligned}\Delta E(\beta_c) &= U(\hat{\beta}) - U(\beta_c) \\ &= A(\beta_c - \hat{\beta})\ln|\hat{\beta} - \beta_c|/\tanh\beta_c \\ &\simeq \tau_Q^{-1/3}\ln(\tau_Q/\tau_0).\end{aligned} \quad (10)$$

Here, $\tau_0 \simeq 1$ is a constant. We can see that, up to a subleading logarithmic correction, the KZ scale of energy is $\simeq \tau_Q^{-1/3}$. Accordingly, in Fig. 4(b) we show a scaled excitation energy $\tau_Q^{1/3}(E - U)$ as a function of scaled time $t/\hat{t}$. For $\tau_Q \gg 1$ the plots for different τ_Q collapse in the KZ regime, $-1 < t/\hat{t} < 1$. There is no collapse at later times when the phase ordering kinetics [93] brings in new physics beyond the KZ mechanism. Having seen how the excitations build up, we can have a closer look at the ferromagnetic correlator,

$$C_R(t) = \langle \sigma_i^z \sigma_j^z \rangle - \langle \sigma_i^z \rangle \langle \sigma_j^z \rangle. \quad (11)$$

Here, the sites i and j are separated by a distance R along one of the axes and the average is taken in the state at time t. Figure 5 shows the scaled correlator $\hat{\xi}^\eta C_R$ as a function of the scaled distance $R/\hat{\xi}$ for three scaled times $t/\hat{t} = -1, 0, 1$. Here, $\hat{\xi} = \tau_Q^{1/3}$ is the scale of length in Eq. (2) and $\hat{t} = \hat{\xi}^z = \tau_Q^{1/3}$ is the scale of time in Eq. (3). In accordance with the scaling hypothesis (4), for each scaled time the plots with different τ_Q collapse to a common scaling function when τ_Q is large enough. The plot for the longest $\tau_Q = 2^{15}$ is practically equal to the scaling function $F(t/\hat{t}, R/\hat{\xi})$.

Comparing the three panels in Fig. 5 we can see that (at odds with the impulse approximation) the range of correlations increases several times between $-\hat{t}$ and $\hat{t}$. This observation is further corroborated by Fig. 6(a) where we collect scaled plots for $\tau_Q = 2^{15}$ at different scaled times. Using $\hat{\xi}$ as a natural unit of length, this figure shows how the correlation spreads in the KZ regime between $-\hat{t}$ and $+\hat{t}$.

Figure 6(b) shows how a scaled range of the correlator in Fig. 6(a) depends on the scaled time $s = t/\hat{t}$. Here, the range is defined as the distance at which the scaled correlator falls below a threshold—set here at 0.1. The nearly linear time dependence is fitted with a line whose slope estimates the scaled velocity of correlation spreading. We repeated the same procedure for thresholds down to 0.02 (below 0.02 the tail of the correlator becomes too noisy for an unambiguous estimation of the correlation range). The estimated slopes/velocities are collected in Fig. 6(c). The velocity increases rather slowly with a decreasing threshold. In the limit of zero threshold—probing the longest correlation tail—it extrapolates to 0.93. We can conclude that the speed limit in this model is $\hat{v}$, which allows the size of the sonic horizon to expand with

$$2\hat{v} = 0.93\frac{\hat{\xi}}{\hat{t}} = 0.93\tau_Q^{-1/2}. \quad (12)$$

In natural units, in accordance with the KZ prediction in Eq. (6), the speed limit becomes slower for slower quenches.

III. EXTENDED QUANTUM XY CHAIN: $z = 3$

We step into the quantum realm with the extended quantum XY periodic spin chain,

$$\begin{aligned}H = -\sum_{n=1}^{N}\big[&(1-\epsilon)\sigma_n^z + J^{xx}\sigma_n^x\sigma_{n+1}^x + J^{yy}\sigma_n^y\sigma_{n+1}^y \\ &+ J^{xzx}\sigma_n^x\sigma_{n+1}^z\sigma_{n+2}^x + J^{yzy}\sigma_n^y\sigma_{n+1}^z\sigma_{n+2}^y\big],\end{aligned} \quad (13)$$

a generalization of the quantum XY chain. It combines the desired $z > 1$ with exact solvability. Here, we consider an anisotropic model,

$$(J^{xx}, J^{yy}, J^{xzx}, J^{yzy}) = \left(a\frac{1+\gamma}{2}, a\frac{1-\gamma}{2}, b\frac{1+\delta}{2}, b\frac{1-\delta}{2}\right), \quad (14)$$

with the external magnetic field parametrized by $\epsilon \in [-1, 1]$. The parameter is driven linearly (1) from an initial $\epsilon = -1$ in the paramagnetic phase, across the critical point at $\epsilon = 0$, to a final $\epsilon = 1$ in the ferromagnetic phase. After the Jordan-Wigner and Fourier transformations (A1) and (A4),
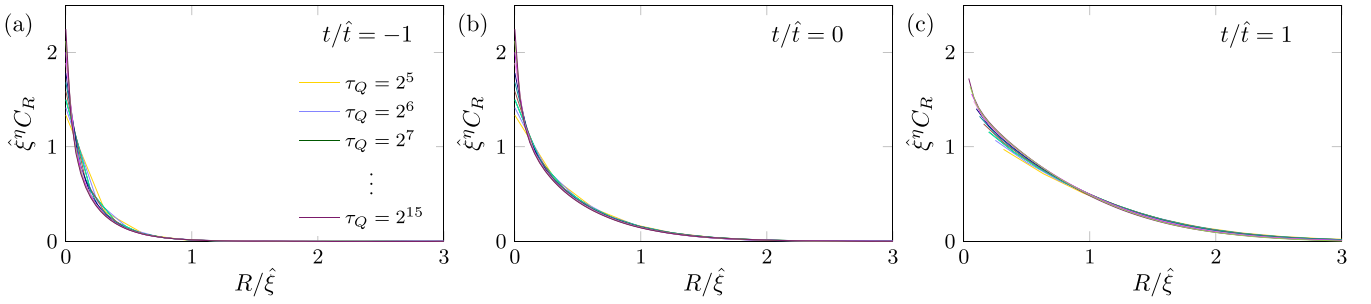
FIG. 5. Classical Ising model in 2D. The scaled correlator $\hat{\xi}^\eta C_R$ as a function of the scaled distance $R/\hat{\xi}$ for scaled times $t/\hat{t} = -1, 0, 1$ (left to right) and different quench times τ_Q. For each scaled time, when $\tau_Q \gg 1$ the plots with different τ_Q collapse to a single scaling function $F(t/\hat{t}, R/\hat{\xi})$, demonstrating the KZ scaling (4) hypothesis for slow enough quenches.

the Hamiltonian becomes

$$H = \sum_{k>0} A_k(\epsilon)(c_k^\dagger c_k + c_{-k}^\dagger c_{-k}) + B_k(c_k c_{-k} + c_{-k}^\dagger c_k^\dagger), \quad (15)$$

where

$$A_k(\epsilon) = 1 - \epsilon - a \cos k - b \cos 2k,$$
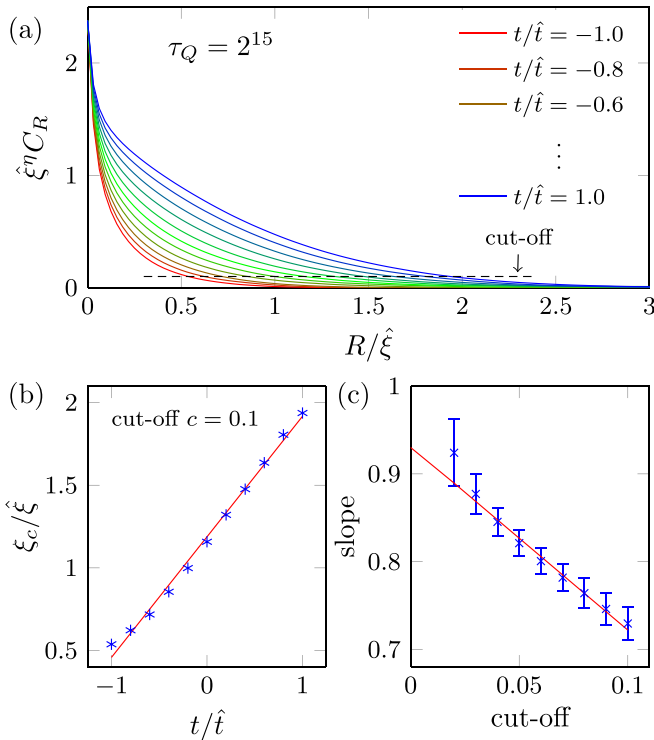$$B_k = a\gamma \sin k + b\delta \sin 2k. \quad (16)$$

FIG. 6. Classical Ising model in 2D. In (a), the scaled correlator $\hat{\xi}^\eta C_R$ as a function of the scaled distance $R/\hat{\xi}$ for $\tau_Q = 2^{15}$ at different scaled times $t/\hat{t} \in [-1, 1]$. The dashed line marks a cutoff c (here, $c = 0.1$) whose crossing point is a working definition of a scaled correlation range $\xi_c/\hat{\xi}$. In (b), the scaled correlation range $\xi_c/\hat{\xi}$ as a function of the scaled time $t/\hat{t}$ for the cutoff $c = 0.1$. The best linear fit yields a slope 0.72 as an estimate of the scaled velocity. In (c), the scaled velocity (slope) as a function of the cutoff. A linear extrapolation to zero cutoff yields 0.93. This number is an estimate for (scaled) velocity at which the furthest correlation tail is spreading.
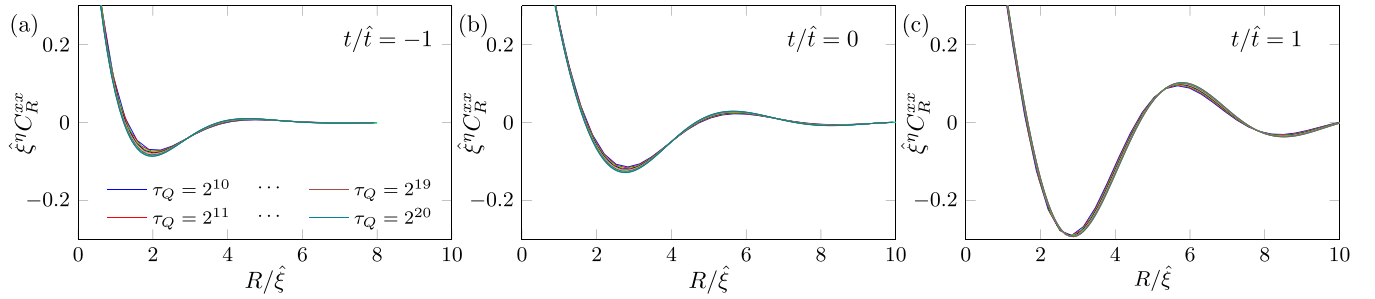
It is diagonalized by eigenmodes of the stationary Bogoliubov–de Gennes equations,

$$\omega_k \begin{pmatrix} U_k \\ V_k \end{pmatrix} = 2[\sigma^z A_k(\epsilon) + \sigma^x B_k] \begin{pmatrix} U_k \\ V_k \end{pmatrix}, \quad (17)$$

with eigenfrequencies $\omega_k = 2\sqrt{A_k^2(\epsilon) + B_k^2}$. Here, we set $a = 4/3$, $b = -1/3$, $\gamma = 1/2$, $\delta = 1$. For the critical $\epsilon = 0$, we obtain a cubic dispersion relation

$$\omega_k \simeq |k|^3, \quad (18)$$

expanding ω_k around $k = 0$, and the dynamical exponent $z = 3$. On the other hand, setting $k = 0$ and expanding in small ϵ, we obtain the gap opening as $\omega_0 \simeq |\epsilon|^1$. Hence $z\nu = 1$ and $\nu = 1/3$. The dominant static ferromagnetic correlations have oscillatory tails,

$$C_R = \langle \sigma_i^x \sigma_{i+R}^x \rangle - \langle \sigma_i^x \rangle \langle \sigma_{i+R}^x \rangle \sim R^{-\eta} e^{-R/\xi} \cos(bR/\xi + c). \quad (19)$$

Here, $\xi \sim |\epsilon|^{-\nu}$ is a static correlation length and $\eta = 1/4$. Given the exponents z and ν, we can define the dynamical length scales (2) and timescales (3), $\hat{\xi} = \tau_Q^{1/6}$ and $\hat{t} = \tau_Q^{1/2}$, respectively. The fastest excited quasiparticles have velocity $\hat{v} \simeq \tau_Q^{-1/3}$ [see Eq. (6)].

The time-dependent quench is solved in Appendix C in a standard way [44] by mapping to the Landau-Zener problem (see Appendix B). The KZ scaling hypothesis (4) is demonstrated in Fig. 7 by a collapse of the plots for different τ_Q. A perfect collapse requires very large $\tau_Q \simeq 2^{20}$, as explained by Eq. (C4). The oscillatory behavior of C_R in the original paramagnetic phase survives through the transition. In order to estimate the range of the scaled correlators, in Fig. 7 we fit their tails with oscillatory functions of the form

$$\hat{\xi}^{1/4} C_R(t) = a(R/\hat{\xi})^{-1/4} e^{-\frac{R/\hat{\xi}}{\xi/\hat{\xi}}} \cos(bR/\hat{\xi} + c), \quad (20)$$

where a, b, c and $\xi/\hat{\xi}$ are the fitting parameters. We are interested how fast the scaled correlation length $\xi/\hat{\xi}$ grows with the scaled time $t/\hat{t}$. In order to reveal the universal behavior undisturbed by any short-range effects, we perform the fit in the range of scaled distances $R/\hat{\xi} > 2.5$. Ferromagnetic correlations for different scaled times $t/\hat{t}$, together with the fits, are shown in Fig. 8(a) (for $\tau_Q = 2^{20}$). The correlation length $\xi/\hat{\xi}$ as a function of scaled time is shown in Fig. 8(b). Its slope, equal to 0.838, provides an estimate of the scaled velocity

FIG. 7. Extended quantum XY chain. Scaled ferromagnetic correlations C_R^{xx} as a function of scaled distance $R/\hat{\xi}$ for the extended XY model in (13) plotted for different quench times τ_Q and at different scaled times $t/\hat{t} = -1, 0, 1$. For large enough τ_Q plots collapse towards a universal scaling function $F(t/\hat{t}, R/\hat{\xi})$, demonstrating the KZ scaling hypothesis (4).

at which the correlations are spreading. For completeness, in Fig. 8(c) we plot the derivative of the plot in Fig. 8(b) with respect to the scaled time. Its maximal value is shown in Fig. 8(d) as a function of $\tau_Q \in [2^{10}, 2^{20}]$. For large τ_Q it extrapolates to

$$2\hat{v} = 0.868 \frac{\hat{\xi}}{\hat{t}} = 0.868 \, \tau_Q^{-1/3}. \tag{21}$$

As in the classical 2D Ising model, where also $z > 1$, the correlation spreading becomes slower for slower quenches.

IV. RANDOM ISING MODEL

In order to break the translational invariance and impede the propagation of excited quasiparticles that could spread correlations, next we consider the random Ising model (RIM) in one dimension defined by the Hamiltonian

$$H = -\sum_{n=1}^{N} \left[(h_n - \epsilon)\sigma_n^z + J_n \sigma_n^x \sigma_{n+1}^x \right]. \tag{22}$$

Here, both transverse fields h_n's and nearest-neighbor couplings J_n's are randomly selected from a uniform distribution between 0 and 1. The quantum critical point at $\epsilon = 0$ is separating the paramagnetic phase ($\epsilon < 0$) from the ferromagnetic one ($\epsilon > 0$). The critical point in this model is surrounded by

Griffiths region [94–96], where the presence of the so-called rare regions primarily manifests in two features: the activated dynamical scaling (the dynamical exponent $z \to \infty$) at the quantum critical point and the existence of singular regions where the linear susceptibility diverges even away from the critical point. The locally ordered rare regions act as giant spins that flip as a whole and are responsible for the exponentially slow dynamics near the critical point. These features are encapsulated in a dynamical exponent that diverges at the critical point as $z \sim |\epsilon|^{-1}$ (see Refs. [97,98] which also show that the correlation length exponent is $\nu = 2$). The average correlation function at criticality is a power law [99],

$$C_R^{xx} = \langle \sigma_i^x \sigma_{i+R}^x \rangle \sim R^{-\eta}, \tag{23}$$

where $\eta = \frac{3-\sqrt{5}}{2} \approx 0.38$.

We consider ramping the parameter ϵ linearly as a function of time (1) driving the Hamiltonian from the initial paramagnetic ground state, across the critical point at $t = 0$, into the ordered phase. References [100–102] showed that the KZ correlation length $\hat{\xi}$ of the model varies logarithmically with the quench rate τ_Q,

$$\hat{\xi} = \ln^2{(\tau_Q/a)}, \tag{24}$$

when $\ln{(\tau_Q/a)} \gg 1$. Here, $a \simeq 1$ is a nonuniversal constant. We can see that the dependence on τ_Q is very weak compared
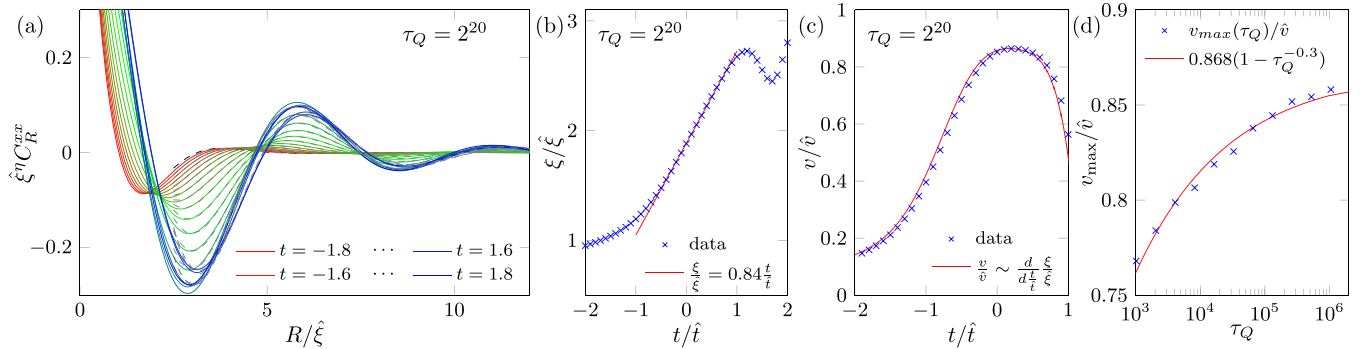

FIG. 8. Extended quantum XY chain. In (a), function (20) is fitted (dashed lines) to the scaled ferromagnetic correlators $\hat{\xi}^{1/4} C_R^{xx}$ for different scaled times during the nonadiabatic stage of the evolution, $t/\hat{t} \in [-2, 2]$. Here, $\tau_Q = 2^{20}$. In (b), the fits provide the scaled correlation length $\xi/\hat{\xi}$ plotted against the scaled time $t/\hat{t}$. The slope of this plot is an estimate of the scaled velocity $v/\hat{v} = 0.84$ at which the correlations are spreading. In (c), a more accurate approximation of the velocity is obtained by taking a derivative of the plot (b) with respect to the scaled time, which yields the scaled velocity $v/\hat{v}$ as a function of the scaled time. Maximal velocity is $v_{\max}/\hat{v} = 0.84$ for $\tau_Q = 2^{20}$. In (d), the maximal velocity is shown as a function of τ_Q. The red line is a fit, which, for large τ_Q, saturates at $v_{\max}/\hat{v} = 0.868$.

to any of the usual KZ power-law scalings (2). Taking into account that the correlation length exponent near the critical point is $\nu = 2$, we get an estimate of the characteristic timescale,

$$\hat{t} = \frac{\tau_Q}{\ln(\tau_Q/a)}, \quad (25)$$

for $\ln(\tau_Q/a) \gg 1$.

In order to solve the dynamics, we map the Hamiltonian by the Jordan-Wigner transformation (A1) to a quadratic spinless free-fermionic model,

$$H = \sum_n (h_n - \epsilon)c_n^\dagger c_n - J_n c_n^\dagger c_{n+1} - J_n c_{n+1} c_n + \text{H.c.} \quad (26)$$

Following the convention of this paper, we confine ourselves to the subspace of even parity of c quasiparticles (antiperiodic boundary conditions, i.e., $c_{N+1} = -c_1$), and in this subspace, we diagonalize the Hamiltonian by a Bogoliubov transformation,

$$c_n = \sum_{m=1}^N (U_{nm}\gamma_m + V_{nm}^* \gamma_m^\dagger). \quad (27)$$

The index m labels the (Bogoliubov) eigenmodes of the stationary Bogoliubov–de Gennes equation

$$\omega_m U_{n,m}^\pm = 2h_n U_{n,m}^\mp - 2j_{n-1} U_{n-1,m}^\mp, \quad (28)$$

where $\omega_m > 0$, $U_{nm}^\pm = U_{nm} \pm V_{nm}$, and antiperiodic boundary conditions ($U_{N+1,m}^\pm = -U_{1,m}^\pm$, $U_{0,m}^\pm = -U_{N,m}^\pm$) are implemented. The eigenstates (U_{nm}, V_{nm}) with positive energy $\omega_m > 0$ normalized so that $\sum_n(|U_{nm}|^2 + |V_{nm}|^2) = 1$, define quasiparticle operators $\gamma_m = U_{nm}^* c_n + V_{nm} c_n^\dagger$. We have corresponding negative energy components of the eigenstates labeled $(U_{nm}^{\text{neg}}, V_{nm}^{\text{neg}})$ with energy $-\omega_m$, which defines a quasiparticle operator $\gamma_m^{\text{neg}} = (U_{nm}^{\text{neg}})^* c_n + V_{nm}^{\text{neg}} c_n^\dagger$. The Bogoliubov transformation renders the Hamiltonian to be $H = \sum_{m=1}^N \omega_m(\gamma_m^\dagger \gamma_m - \frac{1}{2})$. In the even parity subspace only states with an even number of quasiparticles belong to the spectrum of H.

In order to find whether the RIM fits into our narrative of the uniform scaled velocity of the correlation spreading by quasiparticles, we proceed with the numerical simulation of the quench. We prepare the initial state of the system deep in the paramagnetic phase in the ground state, i.e., in the Bogoliubov vacuum state for quasiparticles at an initial time t_0 where $\epsilon(t_0) = 5$. As we tune the parameter $\epsilon(t)$ towards 0 [see Eq. (1)], the state of the systems departs from its adiabatic ground state and gets excited due to the closing of the energy gap near the critical point. We work in the Heisenberg picture where we assume that the excited state is a Bogoliubov vacuum while the time dependence is ascribed to a set of time-dependent quasiparticle operators,

$$\gamma_m(t) = u_{nm}^*(t) c_n + v_{nm}^*(t) c_n^\dagger. \quad (29)$$

The Bogoliubov modes u_{nm} and v_{nm} solve the time-dependent Bogoliubov–de Gennes equations

$$i \frac{du_{nm}^\pm}{dt} = 2[h_n - \epsilon(t)]u_{nm}^\mp - 2J_n u_{n\mp1,m}^\mp \quad (30)$$

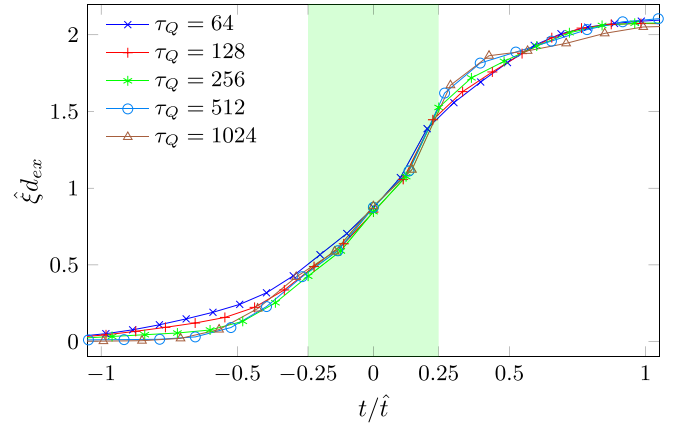We integrate Eq. (30) numerically using the second-order Suzuki-Trotter method (see Appendix D). The density of

FIG. 9. Random Ising model. Average scaled density of excitations $\hat{\xi} d_{\text{ex}}$ during the quench as a function of scaled time $t/\hat{t}$ for different quench times τ_Q. Here, we use Eqs. (24) and (25) with $a = 0.118$. This a was tuned to obtain the best possible collapse at $t/\hat{t} = 0$ but the plots collapse well during the whole quench. The KZ diabatic stage (shaded in green) extends roughly from $-0.25t/\hat{t}$ to $0.25t/\hat{t}$. This is where the excitation grows before it saturates in the last adiabatic stage. Averaging was done over 30 random realizations for a lattice of size $N = 128$.

excited Bogoliubov quasiparticles $d_{\text{ex}}(t)$ can be calculated at each time step by projecting the time-dependent Bogoliubov modes $[u_{nm}(t), v_{nm}(t)]$ onto the corresponding instantaneous static negative Bogoliubov modes $(U_{nm}^{\text{neg}}, V_{nm}^{\text{neg}})$,

$$d_{\text{ex}}(t) = \frac{1}{N} \sum_s^N \sum_p^N |\langle U_p^{\text{neg}}, V_p^{\text{neg}} | u_s(t), v_s(t) \rangle|^2. \quad (31)$$

While in the initial adiabatic stage, the system remains in the instantaneous ground state and hence the density of quasiparticle excitations is 0. On tuning the field $\epsilon(t)$ towards its critical value at $t/\hat{t} = 0$, the system gets excited and consequently d_{ex} starts to grow. As we keep increasing the field $\epsilon(t)$, d_{ex} saturates as the system ends its nonadiabatic journey across the critical point. In Fig. 9 we see that the scaled plots (averaged over disorder) for different τ_Q collapse in accordance with the dynamical scaling hypothesis (4).

The hypothesis for correlations in Eq. (4) is verified by a similar collapse of the plots in Fig. 10. We consider large τ_Q as the logarithmic KZ scaling laws are only valid in that regime. The correlation function is averaged over 100 instances of disorder and lattice translations on a lattice of $N = 256$. This lattice is a few times longer than the longest correlation range. The details of calculating the correlation functions are given in Appendix E.

A close look at Fig. 10 reveals that the scaled dynamical correlation function grows with scaled time. In order to appreciate the growth, we collect the scaled correlators for different scaled times in Fig. 11(a). In order to estimate the scaled correlation range $\xi_c/\hat{\xi}$ as a function of scaled time, we choose a cutoff c for the scaled correlation and calculate scaled distances corresponding to the cutoff by spline interpolation. Figure 11(b) shows the scaled range as a function of the scaled time for the cutoff (selected equal to 0.5) in Fig. 11(a). Near the critical point, we approximate it with a linear dependence
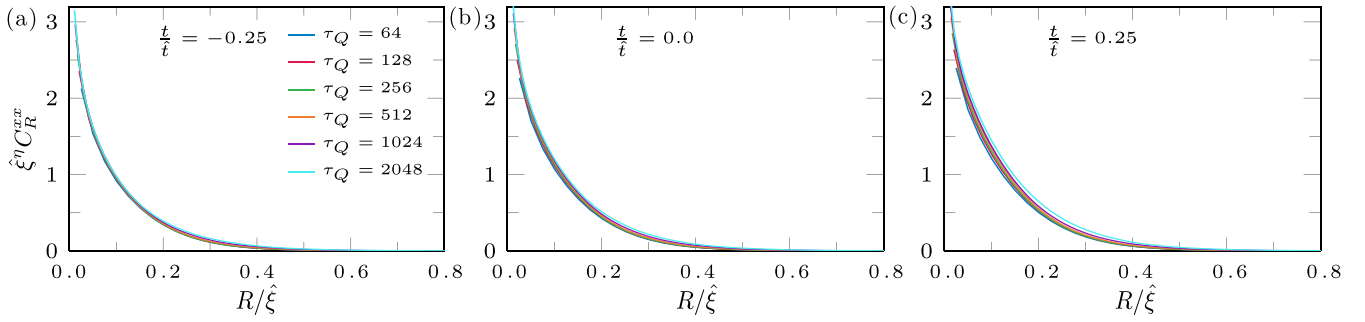
FIG. 10. Random Ising model. Average scaled ferromagnetic correlations $\hat{\xi}^{\eta} C_R^{xx}$ as a function of scaled distance $R/\hat{\xi}$ for the random Ising model (22) plotted for different quench times τ_Q and at different scaled times $t/\hat{t} = -0.25, 0, 0.25$. For large enough τ_Q plots collapse towards a universal scaling function $F(t/\hat{t}, R/\hat{\xi})$, demonstrating the KZ scaling hypothesis (4).

where the slope is $0.113\hat{\xi}/\hat{t}$. We repeat the same procedure for other cutoffs. We present the enumerated slopes for various cutoffs in Fig. 11(c), with the error bars indicating the fitting error. Finally, we estimate the sonic horizon expansion speed in this model with the maximal observed value

$$2\hat{v} = 0.12\frac{\hat{\xi}}{\hat{t}} = 0.12\frac{\ln^3(\tau_Q/a)}{\tau_Q}. \qquad (32)$$

Compared to the previous models, with the prefactor 0.12, the speed limit is significantly below expectations in this
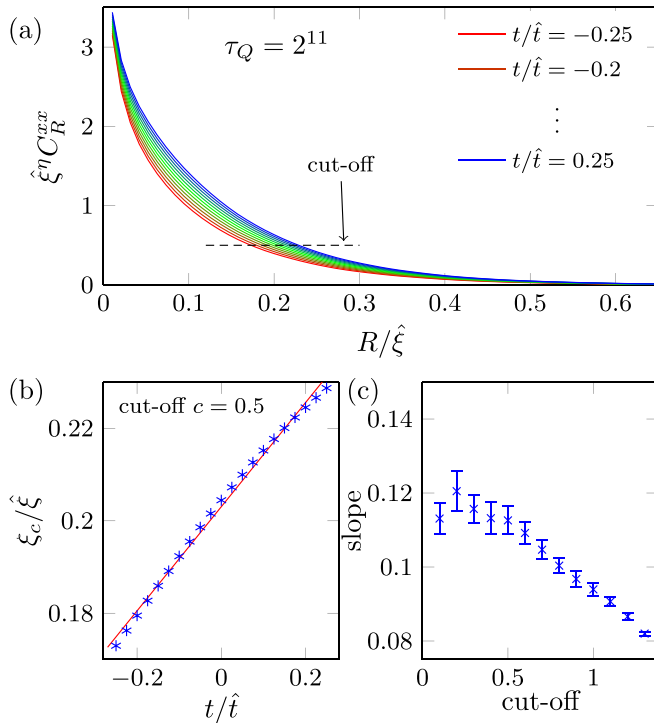

FIG. 11. Random Ising model. In (a), the scaled correlator $\hat{\xi}^{\eta} C_R$ as a function of the scaled distance $R/\hat{\xi}$ for $\tau_Q = 2^{11}$ at different scaled times $t/\hat{t}$ in $[-0.25, 0.25]$. The dashed line marks a cutoff (here, 1) whose crossing point is a working definition of a scaled correlation range $\xi_c/\hat{\xi}$. In (b), the scaled correlation range $\xi_c/\hat{\xi}$ as a function of the scaled time $t/\hat{t}$ for the cutoff $c = 0.5$. The best linear fit yields a slope of 0.113 as an estimate of the scaled velocity. In (c), the scaled velocity (slope) as a function of the cutoff, with the error bars indicating fitting errors.

case. The entangled Bogoliubov quasiparticles get excited but, due to their localization by disorder, they do not propagate to spread correlations appreciably. In the spin language, the locally ordered regions are excited, but they essentially stay where they are. One may even argue that in this case, the adiabatic-impulse-adiabatic freeze-out approximation captures the essential physics.

V. LONG-RANGE EXTENDED ISING MODEL: $0 < z < 1$

The long-range extended Ising model is a further generalization of the extended XY model that we have discussed in Sec. III. Now the Hamiltonian of the system includes not only the nearest-neighbor and next-nearest-neighbor interactions, but all possible long-range cluster terms,

$$H = -\sum_{n=1}^{N}\left[(1-\epsilon)\sigma_n^z + \sum_{r=1}^{N-1}J_r\sigma_n^x\sigma_{n+r}^x\prod_{i=n+1}^{n+r-1}\sigma_i^z\right]. \quad (33)$$

Here,

$$J_r = \frac{1}{\zeta(\alpha)}\frac{1}{r^{\alpha}}, \qquad (34)$$

and the normalization by the Riemann zeta function, possible for $\alpha > 1$, is such that $\sum_r J_r = 1$. The case of $\alpha > 2$ is not the most interesting here because the model behaves effectively as the short-range one [103–107]. Similarly, when $0 \leqslant \alpha \leqslant 1$ we would need to restrict ourselves to a finite system because the thermodynamic limit does not exist in this case, and the model behaves effectively as the Lipkin-Meshkov-Glick model [108] with infinite-range interactions. Therefore, we focus here on the intermediate $1 < \alpha < 2$, where a crossover between the short and infinite ranges happens. In this regime, we consider the linear quench (1) driving the system from the initial paramagnetic phase at $t = -\infty$, across the critical point at $t = 0$, to the final ferromagnetic phase.

Owing to the string operator in the long-range interaction terms, the model can be mapped to a quadratic free fermion model and solved analytically. After the Jordan-Wigner transformation (A1) the Hamiltonian (33) becomes

$$H = -\sum_n(1-\epsilon)(c_n c_n^{\dagger} - c_n^{\dagger} c_n)$$

$$-\sum_{n,r}J_r(c_n^{\dagger}c_{n+r} + c_n^{\dagger}c_{n+r}^{\dagger} + \text{H.c.}), \quad (35)$$
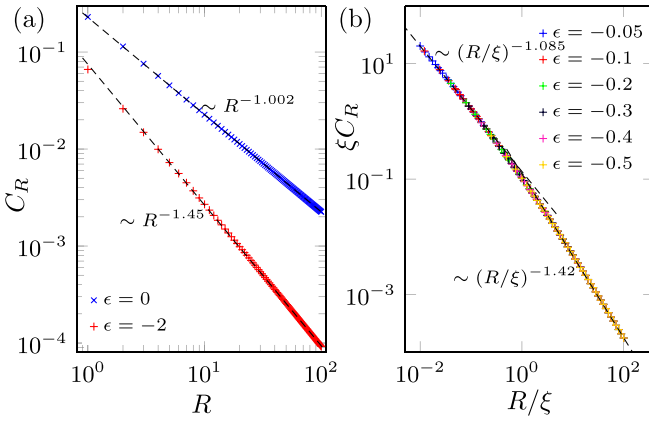
FIG. 12. Long-range extended Ising model. In (a), the static correlation function C_R at the critical $\epsilon = 0$ for $\alpha = 3/2$. The solid line is a linear fit with a slope $-1.002 \approx -1$. The same panel shows the same function far from the critical point at $\epsilon = -2$. The solid line is a linear fit with a slope $-1.45 \approx -(3 - \alpha)$. In (b), the scaled static correlation function ξC_R as a function of scaled distance R/ξ. In accordance with the static scaling hypothesis (39), the plots for different ϵ collapse to a unique scaling function. We can see a crossover from the critical $(R/\xi)^{-1}$ to the off-critical $(R/\xi)^{-3/2}$ near $R/\xi = 1$. The straight lines are linear fits with slopes $-1.085 \approx -1$ and $-1.42 \approx -(3 - \alpha)$ for smaller and larger R/ξ, respectively.

for the antiperiodic boundary conditions. This representation is also known as the long-range Kitaev model [103,104], where the hopping and pairing terms are of equal strength. After Fourier transformation (A4),

$$H = -2 \sum_{k>0} [1 - \epsilon - \mathrm{Re}(\tilde{J}_k)](c_k^\dagger c_k + c_{-k}^\dagger c_{-k})$$
$$+ \mathrm{Im}(\tilde{J}_k)(c_k^\dagger c_{-k}^\dagger + c_{-k} c_k), \qquad (36)$$

where $\mathrm{Re}(\tilde{J}_k)$ and $\mathrm{Im}(\tilde{J}_k)$ are, respectively, the real and imaginary parts of the Fourier transform $\tilde{J}_k = \sum_r J_r e^{ikr}$. We have $\tilde{J}_k = \frac{\mathrm{Li}_\alpha(e^{ik})}{\zeta(\alpha)}$, where Li is the polylogarithm function $\mathrm{Li}_\alpha(x) = \sum_{n=1}^{\infty} \frac{x^n}{n^\alpha}$.

We can now find the stationary Bogoliubov–de Gennes equations (17) with $A_k(\epsilon) = 1 - \epsilon - \mathrm{Re}(\tilde{J}_k)$, $B_k = \mathrm{Im}(\tilde{J}_k)$, and eigenfrequencies $\omega_k = 2\sqrt{A_k^2(\epsilon) + B_k^2}$. We have a critical point at $\epsilon = 0$ where the gap closes for $k = 0$. Another critical point, not to be considered here, is at $\epsilon = 2(1 - 2^{-\alpha})$ and $k = \pi$. The dispersion relation at the critical $\epsilon = 0$ is

$$\omega_k \simeq |k|^{\alpha-1}, \qquad (37)$$

hence the dynamical exponent is $z = \alpha - 1 \in (0, 1)$. On the other hand, for small ϵ, the gap at $k = 0$ closes as $\omega_0 = 2|\epsilon|$, hence $z\nu = 1$.

In a short-range model for large R the correlation function decays exponentially with R when the system is away from the critical point, but this does not need to hold for long-range interactions. Indeed, our system has a power-law scaling even far away from the critical point [103,104],

$$C_R = \langle \sigma_i^x \sigma_{i+1}^z \cdots \sigma_{i+R-1}^z \sigma_{i+R}^x \rangle \sim 1/R^{3-\alpha} \qquad (38)$$

[compare Fig. 12(a)]. On the other hand, as discussed in more detail in Ref. [109], at the critical point we expect a

critical power law $C_R \sim 1/r^\eta$ with $\eta < \alpha$. Indeed, in Fig. 12(a) we find that $\eta = 1$ for $\alpha = 3/2$. Similarly as for short-range interactions, for a small ϵ we expect a crossover between the two power laws when R is close to $\xi \sim \epsilon^{-\nu}$. Note that here ξ is not the usual exponential correlation length, even though it scales with ϵ in the characteristic way. The crossover can be verified with a static scaling hypothesis,

$$\xi^\eta C_R = F_{\mathrm{st}}(R/\xi). \qquad (39)$$

With $\xi = \epsilon^{-\nu}$ the plots of the scaled correlator $\xi^\eta C_R$ as a function of the scaled distance R/ξ for different ϵ should collapse to a common static scaling function $F_{\mathrm{st}}(x)$. We expect $F_{\mathrm{st}}(x)$ to cross over around $x = 1$ between the critical tail x^{-1} for small x and $x^{3-\alpha}$ for large x. Indeed, this is what we see in Fig. 12(b). The unscaled leading static tail is, therefore,

$$C_R \simeq \xi^{1/2} R^{-3/2} \qquad (40)$$

for $R \gg \xi$.

Having verified the static hypothesis, we are encouraged to propose its dynamical version in the same form (4) as for local interactions. The dynamics is described by the time-dependent Bogoliubov–de Gennes equations (C1) whose solution is presented in Appendix F. The KZ mechanism has recently been verified in a similar model [61], where the defect density was found to scale as $\tau_Q^{-1/2(\alpha-1)}$, in agreement with the KZ prediction $\tau_Q^{-\nu/(1+z\nu)}$ (see also Ref. [110]). Further developments, such as the scaling of excitation energy (consistent with KZ) or possible experimental implementation, were considered in Refs. [111,112]. Here, we are interested in the buildup of correlations during the quench. In Fig. 13(a) we show scaled correlation functions at different scaled times. For definiteness, in this figure we set $\hat{t} = \tau_Q^{1/2}$ and $\hat{\xi} = \tau_Q^{1/2(\alpha-1)}$ with both numerical prefactors equal to 1. We can see that up to $t = 0.35\hat{t}$ the scaled correlators for different τ_Q collapse, demonstrating the KZ scaling hypothesis in Eq. (4). At $t/\hat{t} \approx 0.4$ they already fail to collapse, signaling the end of the KZ regime and the beginning of phase ordering in the second adiabatic stage.

In Fig. 14(a), we collect scaled correlators for different scaled times, $s = t/\hat{t}$, in the KZ regime. In order to gain better insight, in Fig. 14(b) we fit their tails with a function

$$\hat{\xi} C_R(s) = A(s)(R/\hat{\xi})^{-3/2} + B(s)(R/\hat{\xi})^{-2} + C(s)(R/\hat{\xi})^{-5/2}.$$

$$(41)$$

Its form is motivated by correlation tails after a sudden quench considered in Appendices G and H. Here, the coefficients A, B, C are functions of the scaled time shown in Fig. 14(c). On top of the leading $A(s)$ tail, subleading dynamical correlations build up in time, with $B(s)$ growing negative and $C(s)$ positive. Their behavior is similar to what is observed after a sudden quench to the critical $\epsilon = 0$ either from $\epsilon = -\infty$ or $\epsilon = -1$ (see Appendices G and H, respectively). The main Fig. 14(b) shows $A(s)$, i.e., the coefficient of the leading long-range tail $\propto R^{-3/2}$.

The same figure shows $A_{\mathrm{ad}}(s)$, i.e., the same coefficient but in case the evolution were adiabatic. $A_{\mathrm{ad}}(s)$ was obtained by a fit to the far tail of the static correlation function at $\epsilon(s) = s/(\tau_Q/\hat{t})$. The same $A_{\mathrm{ad}}(s)$ can be obtained by equating the static tail (40) with the adiabatic tail $C_R = A_{\mathrm{ad}}(s)\hat{\xi}^{1/2}/R^{3/2}$
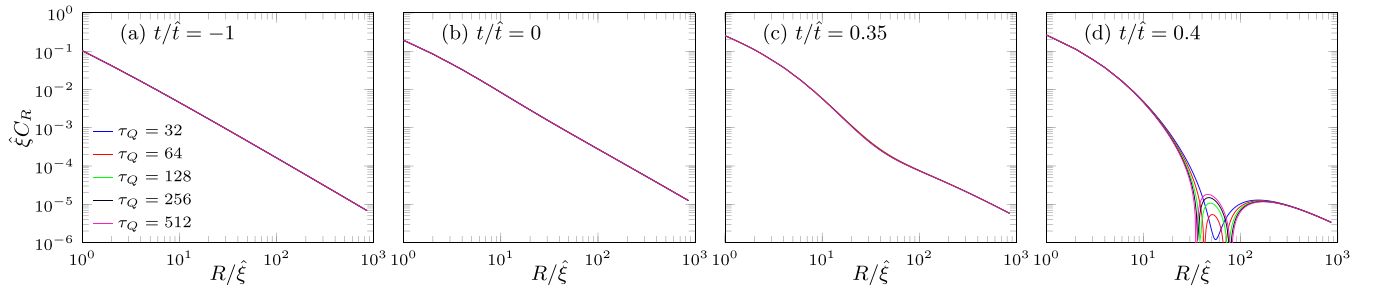
FIG. 13. Long-range extended Ising model. The scaled dynamical correlation function $\hat{\xi}C_R$ for different quench times τ_Q at different scaled times, $s = t/\hat{t}$, during the quench. Here, $\alpha = 3/2$. From left to right: $s = -1, 0, 0.35, 0.4$. In (a) at $s = -1$, the evolution is still adiabatic and the plots for different τ_Q collapse according to the static scaling hypothesis which is equivalent to the KZ hypothesis in this early adiabatic regime. In (b) at $s = 0$, when crossing the critical point, the evolution is diabatic. Different τ_Q collapse to a common scaling function $F(s, R/\hat{\xi})$, in accordance with the KZ scaling hypothesis (4). In (c) at $s = 0.35$, the correlation function begins to bend down at distances between $R/\hat{\xi} = 10$ and 100. Different τ_Q collapse, as the evolution is still in the KZ regime. Finally, in (d) at $s = 0.4$, the collapse fails due to the phase ordering after the system left the KZ regime and entered the adiabatic one. At the distances between $R/\hat{\xi} = 10$ and 100 the correlations become negative for longer τ_Q.

[compare (41)],

$$A_{\mathrm{ad}}(s) \simeq \left[\frac{\xi(s)}{\hat{\xi}}\right]^{1/2} \simeq \left[\frac{\epsilon(s)^{-\nu}}{\hat{\xi}}\right]^{1/2} \sim s^{-\nu/2}. \quad (42)$$

Here, $A_{\mathrm{ad}}(s) \sim s^{-1}$ for $\alpha = 3/2$ is consistent with the divergence we observe in Fig. 14(b). We can also see that, as expected, $A(s)$ follows $A_{\mathrm{ad}}(s)$ in the initial adiabatic stage up to $s \simeq -1$. After that, in the diabatic KZ stage, it lags behind

as it cannot catch up with the diverging $A_{\mathrm{ad}}(s)$. If it did not, and the evolution were adiabatic, then the correlation range—defined by R where C_R falls below a fixed small cutoff—would diverge near the critical point as $|t|^{-2/3}$.

After $A(s)$ begins to lag behind the adiabatic evolution, it continues to grow at a finite rate until the critical point. This is the stage where the long-range model is the most reminiscent of the standard causal KZ picture. After the critical point $A(s)$ begins to dip down around $s \approx 0.2$, but this is where the KZ scaling hypothesis (4) begins to be violated [see Fig. 13(d)].
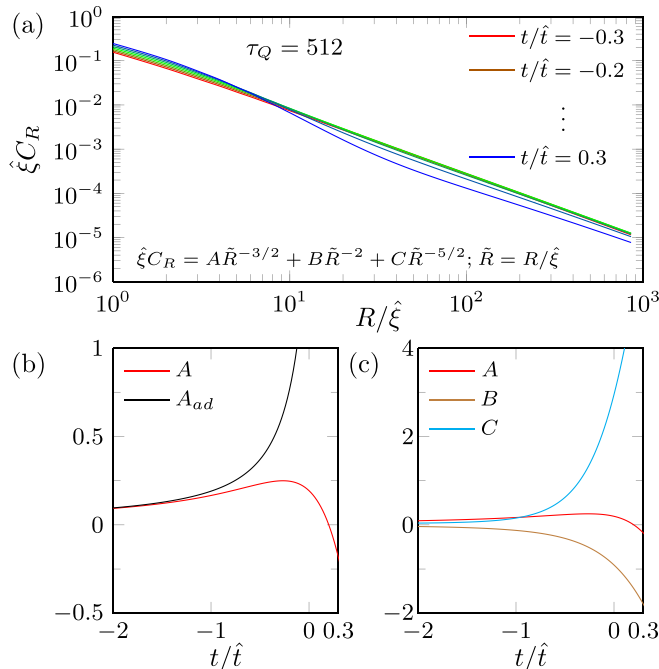
VI. CONCLUSION

We reevaluate the causal/sonic horizon version of the Kibble-Zurek mechanism (KZM). In the initial adiabatic stage of the evolution, the correlation range follows its adiabatic counterpart. At $-\hat{t}$ it begins to lag behind the diverging adiabatic range and continues to grow at a finite rate set by the speed limit $\simeq \hat{\xi}/\hat{t}$. This way, between $-\hat{t}$ and $+\hat{t}$, the correlation range can increase several times, at odds with the impulse approximation where it remains frozen.

There are notable exceptions, such as the random quantum Ising chain, where the increase is small due to localization of excited quasiparticles that prevents them from spreading entanglement. There are interesting generalizations, such as the long-range extended Ising model, where it is the power-law correlation tail, rather than the exponential correlation length, that lags behind its diverging adiabatic evolution.

FIG. 14. Long-range extended Ising model. In (a), scaled correlator $\hat{\xi}C_R$ for $\alpha = 3/2$ as a function of scaled distance for different scaled times in the log-log scale. In (b), in the inset the coefficients A, B, C in Eq. (41) fitted to the tail of the scaled correlator are shown as a function of scaled time $s = t/\hat{t}$. The main picture shows $A(t/\hat{t})$ together with the adiabatic $A_{\mathrm{ad}}(t/\hat{t})$. In the initial adiabatic stage A follows A_{ad}. In the KZ stage A_{ad} diverges to infinity at the critical point, forcing A to lag behind.

APPENDIX A: JORDAN-WIGNER, FOURIER, AND BOGOLIUBOV TRANSFORMATIONS

After the Jordan-Wigner transformation,

$$
\sigma_n^x = -(c_n + c_n^\dagger) \prod_{m<n}(1 - 2c_m^\dagger c_m),
$$
$$
\sigma_n^y = i(c_n - c_n^\dagger) \prod_{m<n}(1 - 2c_m^\dagger c_m), \tag{A1}
$$
$$
\sigma_n^z = 1 - 2c_n^\dagger c_n,
$$

introducing fermionic operators c_n that satisfy $\{c_m, c_n^\dagger\} = \delta_{mn}$ and $\{c_m, c_n\} = \{c_m^\dagger, c_n^\dagger\} = 0$, the Hamiltonian H becomes [91]

$$
H = P^+ H^+ P^+ + P^- H^- P^-. \tag{A2}
$$

Above $P^\pm = \frac{1}{2}[1 \pm P]$ are projectors on subspaces with even (+) and odd (−) parity,

$$
P = \prod_{n=1}^N \sigma_n^z = \prod_{n=1}^N (1 - 2c_n^\dagger c_n), \tag{A3}
$$

and $H^\pm$ are corresponding reduced Hamiltonians. The c_n's in H^- satisfy the periodic boundary condition $c_{N+1} = c_1$, but the c_n's in H^+ are antiperiodic, $c_{N+1} = -c_1$.

The initial ground state at $\epsilon \to -\infty$ has even parity, hence we can confine to the even subspace. The translationally invariant H^+ is diagonalized by a Fourier transform followed by a Bogoliubov transformation [91]. The antiperiodic Fourier transform is

$$
c_n = \frac{e^{-i\pi/4}}{\sqrt{N}} \sum_k c_k e^{ikn}, \tag{A4}
$$

where the pseudomomentum takes half-integer values

$$
k = \pm \frac{1}{2}\frac{2\pi}{N}, \pm\frac{3}{2}\frac{2\pi}{N}, \dots, \pm\frac{N-1}{2}\frac{2\pi}{N}. \tag{A5}
$$

Diagonalization of H^+ is completed by a Bogoliubov transformation,

$$
c_k = U_k \gamma_k + V_{-k}^* \gamma_{-k}^\dagger, \tag{A6}
$$

provided that Bogoliubov modes (U_k, V_k) are eigenstates of stationary Bogoliubov–de Gennes equations with positive eigenfrequency ω_k.

APPENDIX B: LANDAU-ZENER MODEL

The canonical Landau-Zener (LZ) model is

$$
i\frac{d}{dt'}\begin{pmatrix} u_k \\ v_k \end{pmatrix} = \frac{1}{2}\left[-\frac{t'}{\tau_k}\sigma^z + \sigma^x \right]\begin{pmatrix} u_k \\ v_k \end{pmatrix}, \tag{B1}
$$

where τ_k is a transition time. Its solution is

$$
u_k = e^{-\frac{\pi}{16}\tau_k} D_{\frac{1}{4}i\tau_k}(z) e^{i\pi/4}, \tag{B2}
$$
$$
v_k = \frac{1}{2} e^{-\frac{\pi}{16}\tau_k} D_{-1+\frac{1}{4}i\tau_k}(z)\sqrt{\tau_k}. \tag{B3}
$$

Here, $D_m(z)$ is the Weber function with an argument,

$$
z = e^{3\pi i/4}\frac{t'}{\sqrt{\tau_k}} \tag{B4}
$$

(see, for instance, Ref. [113]).

APPENDIX C: TIME-DEPENDENT EXTENDED XY MODEL

The time-dependent problem is

$$
i\frac{d}{dt}\begin{pmatrix} u_k \\ v_k \end{pmatrix} = 2[\sigma^z A_k(t/\tau_Q) + \sigma^x B_k]\begin{pmatrix} u_k \\ v_k \end{pmatrix}. \tag{C1}
$$

It can be mapped to the canonical LZ model where

$$
\tau_k = 4\tau_Q(a\gamma \sin k + b\delta \sin 2k)^2, \tag{C2}
$$

$$
t' = 4\tau_Q(a\gamma \sin k + b\delta \sin 2k)
$$
$$
\times \left(\frac{t}{\tau_Q} - (1 - a\cos k - b\cos 2k) \right). \tag{C3}
$$

Only small quasimomenta up to $\hat{k} \simeq \tau_Q^{-1/6}$ become excited, hence for $k \ll 1$ we can approximate

$$
u_k = e^{-\frac{1}{4}\pi q^2} D_{iq^2}(z) e^{i\pi/4},
$$
$$
v_k = e^{-\frac{1}{4}\pi q^2} D_{-1+iq^2}(z) 2q,
$$
$$
z = 4e^{3\pi i/4}\left(2s - \frac{q^{4/3}3^{1/3}}{\tau_Q^{1/6}} \right), \tag{C4}
$$

where $q = \frac{1}{3}k^3\sqrt{\tau_Q}$ is a scaled quasimomentum and $s = t/\sqrt{\tau_Q}$ is a scaled time. These formulas are consistent with $\hat{\xi} \simeq \tau_Q^{1/6}$ and $\hat{t} \simeq \tau_Q^{1/2}$, respectively.

Only q up to $q \approx 1$ get excited. For them, when τ_Q is large enough, we can further approximate

$$
z = 4e^{3\pi i/4}\left(2s - \frac{q^{4/3}3^{1/3}}{\tau_Q^{1/6}} \right) \approx 8e^{3\pi i/4}s \tag{C5}
$$

and obtain

$$
u_k = e^{-\frac{1}{4}\pi q^2} D_{iq^2}(8e^{3\pi i/4}s) e^{i\pi/4},
$$
$$
v_k = e^{-\frac{1}{4}\pi q^2} D_{-1+iq^2}(8e^{3\pi i/4}s) 2q. \tag{C6}
$$

In accordance with the KZ scaling hypothesis (4), these nonadiabatic modes depend on the scaled variables s and q only. However, the approximation in (C5) requires $\tau_Q^{1/6} \gg 1$, which is why we consider large $\tau_Q \simeq 2^{20}$ in Fig. 8.

APPENDIX D: SOLVING THE TIME-DEPENDENT BOGOLIUBOV–DE GENNES EQUATIONS

The time-dependent problem in Eq. (30) is

$$i\frac{du_{nm}^{\pm}}{dt} = 2[h_n - \epsilon(t)]u_{nm}^{\mp} - 2J_n u_{n\mp1,m}^{\mp}. \tag{D1}$$

The central theme in the time evolution of quantum mechanical states is that of exponentiation of the Hamiltonian which can be attributed to the unitary nature of its dynamics. This becomes notoriously hard when the Hamiltonian consists of noncommuting terms. To add to that, the random Ising model also lacks translational invariance. It renders useless the mapping of time-dependent Bogoliubov–de Gennes equations to the canonical LZ model, unlike the other models used in this paper. Consequently we resort to techniques such as the Suzuki-Trotter (ST) expansion of the exponential which has the desirable feature of conserving the norm of the evolution. The ST approximation deals with approximating the exponential, expressed in terms of the two noncommuting pieces, by a product of exponential. ST of second order can be written as

$$e^{\delta(A+B)} = \lim_{\delta\to0} e^{\frac{\delta}{2}A}e^{\delta B}e^{\frac{\delta}{2}A} + O(\delta)^3.$$

We separate the field part (A) and the coupling part (B) and solve them separately for a small time dt,

$$\text{field:} \quad \begin{pmatrix} u_n^+(t+dt) \\ u_n^-(t+dt) \end{pmatrix} = e^{-iA(t+dt/2)dt}\begin{pmatrix} u_n^+(t) \\ u_n^-(t) \end{pmatrix},$$

$$\text{coupling:} \quad \begin{pmatrix} u_{n+1}^+(t+dt) \\ u_n^-(t+dt) \end{pmatrix} = e^{-iBdt}\begin{pmatrix} u_{n+1}^+(t) \\ u_n^-(t) \end{pmatrix},$$

where $A(t) = [h_n - \epsilon(t)]\sigma_x$ and $B = -2J_n\sigma_x$, and drop the index m for convenience. We begin our quench at $\epsilon(t) = 5$.

APPENDIX E: CALCULATION OF TWO-SITE CORRELATION FUNCTION IN THE RANDOM ISING MODEL

Let us define two operators a_i and b_i in terms of fermionic operators as $a_i = c_i^\dagger + c_i$ and $b_i = c_i^\dagger - c_i$. Using the Jordan-Wigner transformation [see (A1)] and Eq. (27), the two-site correlation function along the longitudinal direction can be written as

$$C_R^{xx} = \langle\Psi(t)|\sigma_i^x\sigma_{i+R}^x|\Psi(t)\rangle \tag{E1}$$

$$= \langle b_i a_{i+1} b_{i+1} a_{i+2} \cdots a_{i+R-1} b_{i+R-1} a_{i+R}\rangle, \tag{E2}$$

where $|\Psi(t)\rangle$ is the evolving state. Our final longitudinal correlation looks as

$$\left|C_R^{xx}\right| = \sqrt{\left|\det\left(A_R^{xx}\right)\right|}, \tag{E3}$$

where

$$A_R^{xx} = \begin{bmatrix} \langle a_{i+1}a_{j+1}\rangle & \langle b_i a_{j+1}\rangle \\ \langle a_{i+1}b_j\rangle & \langle b_i b_j\rangle \end{bmatrix}_{i,j=1,...,R}, \tag{E4}$$

and where we redefine $\langle a_i a_i\rangle = \langle b_i b_i\rangle = 0$. Equations (E3) and (E4) follow from (E2) using the Wick theorem. See, for instance, Refs. [114,115] for more details on similar calculations. Finally, two-point correlation functions are obtained as

$$\langle a_i a_j\rangle = \sum_m u_{im}^+ u_{jm}^{+*},$$

$$\langle a_i b_j\rangle = \sum_m u_{im}^+ u_{jm}^{-*},$$

$$\langle b_i a_j\rangle = -\sum_m u_{im}^- u_{jm}^{+*},$$

$$\langle b_i b_j\rangle = -\sum_m u_{im}^- u_{jm}^{-*},$$

where $\sum_m$ denotes the summation over all Bogoliubov modes.

APPENDIX F: TIME-DEPENDENT LONG-RANGE ISING MODEL

The time-dependent Bogoliubov–de Gennes equations map to the canonical LZ model (B1) where

$$\tau_k = 4\tau_Q \,\text{Im}(\tilde{J}_k)^2,$$

$$t' = 4\tau_Q \,\text{Im}(\tilde{J}_k)\left(\frac{t}{\tau_Q} - 1 + \text{Re}(\tilde{J}_k)\right). \tag{F1}$$

For the relevant $k \ll 1$, its exact solution can be approximated by

$$u_k = e^{-\frac{1}{4}\pi q^2}D_{iq^2}(z)e^{i\pi/4},$$

$$v_k = e^{-\frac{1}{4}\pi q^2}D_{-1+iq^2}(z)q, \tag{F2}$$

$$z = 2e^{3\pi i/4}\left(s - C\frac{q}{\tau_Q}\right),$$

where $C \simeq 1$ is a constant, $q \simeq k^{1/2}\tau_Q^{1/2}$ is a scaled quasi-momentum, and $s = t/\sqrt{\tau_Q}$ a scaled time. These formulas are consistent with the KZ scales $\hat{t} \simeq \tau_Q^{1/2}$ and $\hat{\xi} \simeq \tau_Q$ for $\alpha = 3/2$. When $\tau_Q \gg 1$ we can approximate $z \approx 2e^{3\pi i/4}s$ and the solution depends on the scaled variables only. In this regime we also expect

$$\hat{v} = \hat{\xi}/\hat{t} \simeq \tau_Q^{1/2} \tag{F3}$$

as a relevant velocity of quasiparticles excited during the quench.

With the exact solution, one can calculate the correlation function,

$$C_R = \delta_{R,0} - 2\alpha_R + 2\,\text{Re}(\beta_R), \tag{F4}$$

where $\alpha_R = \frac{1}{\pi}\int_0^\pi dk|u_k|^2\cos kR$ and $\beta_R = \frac{1}{\pi}\int_0^\pi dk\, u_k v_k^*\sin kR$.

APPENDIX G: INFINITE SUDDEN QUENCH FROM $\epsilon = -\infty$ TO THE CRITICAL POINT IN THE LONG-RANGE ISING MODEL

In this and the next Appendix, we consider sudden quenches that have also been considered before in the context of dynamical phase transitions in the Lochschmidt echo [116]. At $\epsilon = -\infty$ (corresponding to infinite transverse field) the ground state—with all spins pointing in $+x$ direction—has no correlations. The correlations begin to build up after a sudden quench at $t = 0$ from $\epsilon = -\infty$ to the critical $\epsilon = 0$. The initial Bogoliubov modes at $t = 0$ are

$$\begin{bmatrix} u_k(0) \\ v_k(0) \end{bmatrix} = \begin{bmatrix} 1 \\ 0 \end{bmatrix}. \tag{G1}$$

After the quench they evolve as

$$\begin{bmatrix} u_k(t) \\ v_k(t) \end{bmatrix} = \begin{bmatrix} U_k^2 e^{-i\omega_k t} + V_k^2 e^{i\omega_k t} \\ U_k V_k (e^{-i\omega_k t} - e^{i\omega_k t}) \end{bmatrix}. \tag{G2}$$

Here, ω_k are the frequencies and (U_k, V_k) the stationary Bogoliubov modes at $\epsilon = 0$. With this solution we can now calculate the correlation function in (F4) consisting of two terms, α_R and β_R.

Let us focus first on α_R. It is useful to notice that

$$|u_k(t)|^2 = 1 + 2U_k^2 V_k^2 (\cos 2\omega_k t - 1)$$

$$= 1 + 2U_k^2 V_k^2 \sum_{n=1}^{\infty} (-1)^n \frac{(2\omega_k t)^{2n}}{(2n)!}. \tag{G3}$$

Correlations at the largest distances R are provided by pairs of correlated quasiparticles with the largest velocities. From the spectrum ω_k for $1 < \alpha < 2$ it can be readily seen that the fastest quasiparticles are those with $k \to 0$. Their velocity tends to infinity. For small k we can approximate [117]

$$\text{Im}(\tilde{J}_k) \approx A_\alpha k^{\alpha-1} + C_\alpha k,$$
$$\text{Re}(\tilde{J}_k) \approx B_\alpha k^{\alpha-1} + 1, \tag{G4}$$

where $A_\alpha = \frac{\Gamma(1-\alpha)\cos(\pi\alpha/2)}{\zeta(\alpha)}$, $B_\alpha = \frac{\Gamma(1-\alpha)\sin(\pi\alpha/2)}{\zeta(\alpha)}$, and $C_\alpha = \frac{\zeta(\alpha-1)}{\zeta(\alpha)}$. Using these approximations we obtain the following asymptotes,

$$\omega_k \approx 2\frac{\Gamma(1-\alpha)}{\zeta(\alpha)} k^{\alpha-1},$$
$$U_k^2 V_k^2 \approx C_1^\alpha (1 + C_2^\alpha k^{2-\alpha}), \tag{G5}$$

with $C_1^\alpha = \frac{1}{4}\frac{A_\alpha^2}{A_\alpha^2+B_\alpha^2}$ and $C_2^\alpha = 2(\frac{C_\alpha}{A_\alpha} - \frac{A_\alpha C_\alpha}{A_\alpha^2+B_\alpha^2})$. Inserting (G3) and (G5) we obtain

$$\alpha_R \approx \frac{1}{\pi} \int_0^\pi dk \, |u_k(t)|^2 \cos kR$$

$$\approx \delta_{0,R} + \frac{2}{\pi} \sum_{n=1}^{\infty} (-1)^n \frac{\left(4\frac{\Gamma(1-\alpha)}{\zeta(\alpha)} t\right)^{2n}}{(2n)!}$$

$$\times \left[C_1^\alpha \int_0^\pi k^{2n(\alpha-1)} \cos(kR) dk \right.$$

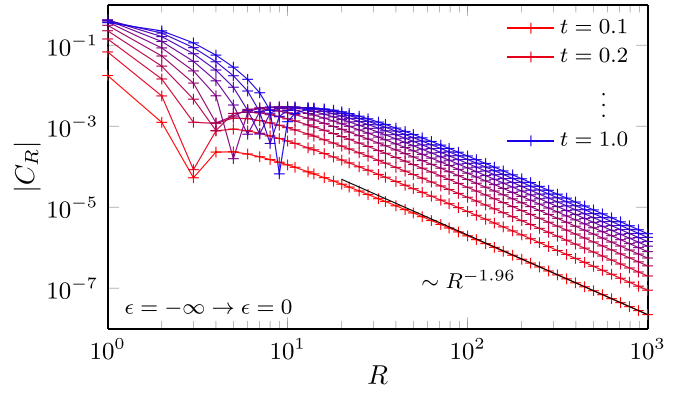$$\left. + C_1^\alpha C_2^\alpha \int_0^\pi k^{2-\alpha+2n(\alpha-1)} \cos(kR) dk \right]. \tag{G6}$$

FIG. 15. Long-range extended Ising model—sudden quench. Spreading of correlation after a sudden quench from $\epsilon = -\infty$ to $\epsilon = 0$. The tail of C_R can be fitted with $R^{-1.96}$, in good agreement with the predicted R^{-2}. C_R changes sign from positive for small R to negative for large R as manifested by the kinks in the plot of $|C_R|$ vs R.

This approximation is valid for large R where the integrals are dominated by small k. For small k the integrand of the second integral is negligible as compared to the first one. By the same token we can neglect all terms except for $n = 1$. For $n = 1$ the first integral is

$$\int_0^\pi k^{2(\alpha-1)} \cos(kR) dk$$

$$= \frac{\pi^{2\alpha-1}}{2\alpha-1} {}_1F_2\left[\alpha - \frac{1}{2}; \frac{1}{2}, \alpha + \frac{1}{2}; -\frac{\pi^2 R^2}{4}\right]$$

$$\approx -\frac{\Gamma(2\alpha-1)\sin[\pi(\alpha-1)]}{R^{2\alpha-1}}. \tag{G7}$$

Here, ${}_1F_2$ is the generalized hypergeometric function [118] and the last approximation is valid for large integer R. Combining (G6) and (G7) we obtain

$$\alpha_R \approx -\frac{2}{\pi} C_1^\alpha \frac{\Gamma[1-\alpha]^2}{\zeta(\alpha)^2} (1 + \cos\pi\alpha) \frac{t^2}{R^{2\alpha-1}}. \tag{G8}$$

For $\alpha = 3/2$ we have $\alpha_R \sim \frac{t^2}{R^2}$.

Performing a similar analysis, for $\alpha = 3/2$ we obtain $\text{Re}(\beta_R) \sim \frac{1}{R^{5/2}}$ which decays faster than α_R. Therefore, in the correlation function (F4), it is α_R that dominates the tail, $C_R \sim \frac{t^2}{R^2}$. In Fig. 15 we show the numerically exact correlation function to confirm the validity of this asymptotic result for large R.

Before the infinite sudden quench, there is no static correlation tail $\sim R^{-3/2}$ to be frozen into the state after the quench. All correlations have to build up dynamically by the spreading of entangled pairs of quasiparticles with opposite quasimomenta excited by the sudden quench. The dynamical correlations develop a negative leading power-law tail $\propto R^{-2}$ and a positive next-to-leading term $\propto R^{-5/2}$. In the next Appendix, we will

see that after a finite quench, similar dynamical correlations build up on top of a frozen static prequench tail $\propto R^{-3/2}$.

APPENDIX H: FINITE SUDDEN QUENCH FROM $\epsilon = -1$ TO THE CRITICAL POINT IN THE LONG-RANGE ISING MODEL

In the previous Appendix, the initial state before the quench was a product state with no correlations. Here, we consider a sudden quench from an initial state at a finite $\epsilon = -1$ where, for $\alpha = 3/2$, the static correlation function decays as $R^{-3/2}$ for large R. Figure 16(a) shows the correlation function at different times after the sudden quench. In Fig. 16(b) we fit its tail with

$$C_R(t) = A(t)R^{-3/2} + B(t)R^{-2} + C(t)R^{-5/2} \qquad \text{(H1)}$$

that includes also two subleading terms. $A(t)$ changes negligibly with respect to its prequench value, comparing to $B(t)$ and $C(t)$. The leading prequench static tail $\propto R^{-3/2}$ remains frozen after the sudden quench.

The buildup of dynamical correlations is captured by the subleading terms. Their initial values are small corrections to the leading prequench static correlator. With time, they evolve away from the initial values such as $\propto t^2$. Similarly as for the infinite sudden quench, $B(t)$ grows negative and $C(t)$ positive. Consequently, the dynamical part on top of the frozen static tail grows positive for small and negative for large R [see Fig. 16(a)].
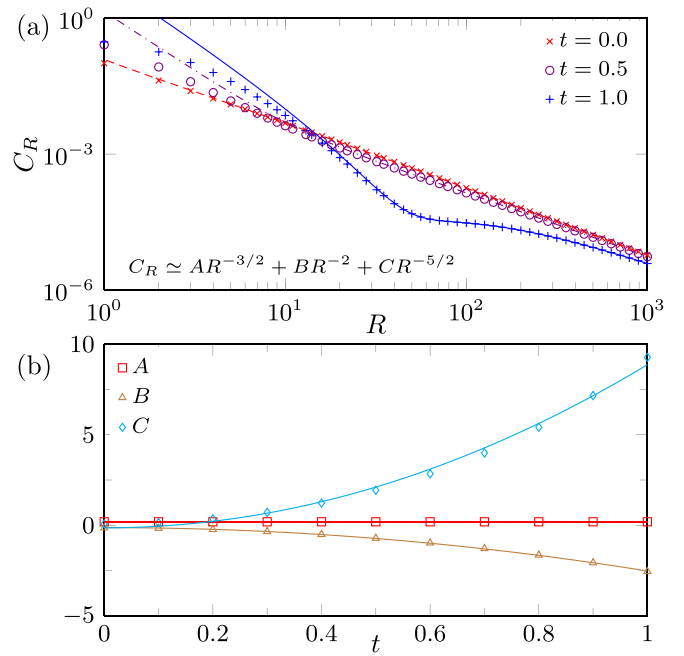

FIG. 16. Long-range extended Ising model—sudden quench. In (a), evolution of the correlations (dots) after a finite sudden quench from $\epsilon = -1$ to the critical $\epsilon = 0$. The correlators are fitted with the formula (H1) in the range $900 < R < 1000$. The fits (solid lines) are plotted in the full range of R. In (b), the coefficients A, B, C in Eq. (H1) as a function of time (dots). Their time dependence is fitted with parabolas $c_0 + c_2 t^2$ (solid lines).

[1] T. W. B. Kibble, J. Phys. A **9**, 1387 (1976); Phys. Rep. **67**, 183 (1980); Phys. Today **60**(9), 47 (2007).

[2] W. H. Zurek, Nature (London) **317**, 505 (1985); Acta Phys. Pol., B **24**, 1301 (1993); Phys. Rep. **276**, 177 (1996).

[3] A. del Campo and W. H. Zurek, Int. J. Mod. Phys. A **29**, 1430018 (2014).

[4] P. Laguna and W. H. Zurek, Phys. Rev. Lett. **78**, 2519 (1997).

[5] A. Yates and W. H. Zurek, Phys. Rev. Lett. **80**, 5477 (1998).

[6] J. Dziarmaga, P. Laguna, and W. H. Zurek, Phys. Rev. Lett. **82**, 4749 (1999).

[7] N. D. Antunes, L. M. A. Bettencourt, and W. H. Zurek, Phys. Rev. Lett. **82**, 2824 (1999).

[8] L. M. A. Bettencourt, N. D. Antunes, and W. H. Zurek, Phys. Rev. D **62**, 065005 (2000).

[9] W. H. Zurek, L. M. A. Bettencourt, J. Dziarmaga, and N. D. Antunes, Acta Phys. Pol., B **31**, 2937 (2000).

[10] M. Uhlmann, R. Schützhold, and U. R. Fischer, Phys. Rev. Lett. **99**, 120407 (2007).

[11] M. Uhlmann, R. Schützhold, and U. R. Fischer, Phys. Rev. D **81**, 025017 (2010).

[12] M. Uhlmann, R. Schützhold, and U. R. Fischer, New J. Phys **12**, 095020 (2010).

[13] E. Witkowska, P. Deuar, M. Gajda, and K. Rzążewski, Phys. Rev. Lett. **106**, 135301 (2011).

[14] A. Das, J. Sabbatini, and W. H. Zurek, Sci. Rep. **2**, 352 (2012).

[15] J. Sonner, A. del Campo, and W. H. Zurek, Nat. Commun. **6**, 7406 (2015).

[16] P. M. Chesler, A. M. García-García, and H. Liu, Phys. Rev. X **5**, 021015 (2015).

[17] I. Chung, R. Durrer, N. Turok, and B. Yurke, Science **251**, 1336 (1991).

[18] M. J. Bowick, L. Chandar, E. A. Schiff, and A. M. Srivastava, Science **263**, 943 (1994).

[19] V. M. H. Ruutu, V. B. Eltsov, A. J. Gill, T. W. B. Kibble, M. Krusius, Y. G. Makhlin, B. Plaçais, G. E. Volovik, and W. Xu, Nature (London) **382**, 334 (1996).

[20] C. Bäuerle, Y. M. Bunkov, S. N. Fisher, H. Godfrin, and G. R. Pickett, Nature (London) **382**, 332 (1996).

[21] R. Carmi, E. Polturak, and G. Koren, Phys. Rev. Lett. **84**, 4966 (2000).

[22] R. Monaco, J. Mygind, and R. J. Rivers, Phys. Rev. Lett. **89**, 080603 (2002).

[23] A. Maniv, E. Polturak, and G. Koren, Phys. Rev. Lett. **91**, 197001 (2003).

[24] C. N. Weiler, T. W. Neely, D. R. Scherer, A. S. Bradley, M. J. Davis, and B. P. Anderson, Nature (London) **455**, 948 (2008).

[25] R. Monaco, J. Mygind, R. J. Rivers, and V. P. Koshelets, Phys. Rev. B **80**, 180501(R) (2009).

[26] D. Golubchik, E. Polturak, and G. Koren, Phys. Rev. Lett. **104**, 247002 (2010).

[27] G. D. Chiara, A. del Campo, G. Morigi, M. B. Plenio, and A. Retzker, New J. Phys. **12**, 115003 (2010).

[28] M. Mielenz, J. Brox, S. Kahra, G. Leschhorn, M. Albert, T. Schaetz, H. Landa, and B. Reznik, Phys. Rev. Lett. **110**, 133004 (2013).

[29] S. Ulm, J. Roßnagel, G. Jacob, C. Degünther, S. T. Dawkins, U. G. Poschinger, R. Nigmatullin, A. Retzker, M. B. Plenio, F. Schmidt-Kaler, and K. Singer, Nat. Commun. **4**, 2290 (2013).

[30] K. Pyka, J. Keller, H. L. Partner, R. Nigmatullin, T. Burgermeister, D. M. Meier, K. Kuhlmann, A. Retzker, M. B. Plenio, W. H. Zurek, A. del Campo, and T. E. Mehlstäubler, Nat. Commun. **4**, 2291 (2013).

[31] S. C. Chae, N. Lee, Y. Horibe, M. Tanimura, S. Mori, B. Gao, S. Carr, and S.-W. Cheong, Phys. Rev. Lett. **108**, 167603 (2012).

[32] S.-Z. Lin, X. Wang, Y. Kamiya, G.-W. Chern, F. Fan, D. Fan, B. Casas, Y. Liu, V. Kiryukhin, W. H. Zurek, C. D. Batista, and S.-W. Cheong, Nat. Phys. **10**, 970 (2014).

[33] S. M. Griffin, M. Lilienblum, K. T. Delaney, Y. Kumagai, M. Fiebig, and N. A. Spaldin, Phys. Rev. X **2**, 041022 (2012).

[34] S. Donadello, S. Serafini, M. Tylutki, L. P. Pitaevskii, F. Dalfovo, G. Lamporesi, and G. Ferrari, Phys. Rev. Lett. **113**, 065302 (2014).

[35] S. Deutschländer, P. Dillmann, G. Maret, and P. Keim, Proc. Natl. Acad. Sci. USA **112**, 6925 (2015).

[36] L. Chomaz, L. Corman, T. Bienaimé, R. Desbuquois, C. Weitenberg, S. Nascimbéne, J. Beugnon, and J. Dalibard, Nat. Commun. **6**, 6162 (2015).

[37] V. Yukalov, A. Novikov, and V. Bagnato, Phys. Lett. A **379**, 1366 (2015).

[38] N. Navon, A. L. Gaunt, R. P. Smith, and Z. Hadzibabic, Science **347**, 167 (2015).

[39] I.-K. Liu, S. Donadello, G. Lamporesi, G. Ferrari, S.-C. Gou, F. Dalfovo, and N. P. Proukakis, Commun. Phys. **1**, 24 (2018).

[40] J. Rysti, S. Autti, G. E. Volovik, and V. B. Eltsov, arXiv:1906.11453.

[41] A. Polkovnikov, Phys. Rev. B **72**, 161201(R) (2005).

[42] B. Damski, Phys. Rev. Lett. **95**, 035701 (2005).

[43] W. H. Zurek, U. Dorner, and P. Zoller, Phys. Rev. Lett. **95**, 105701 (2005).

[44] J. Dziarmaga, Phys. Rev. Lett. **95**, 245701 (2005).

[45] J. Dziarmaga, Adv. Phys. **59**, 1063 (2010).

[46] A. Polkovnikov, K. Sengupta, A. Silva, and M. Vengalattore, Rev. Mod. Phys. **83**, 863 (2011).

[47] R. Schützhold, M. Uhlmann, Y. Xu, and U. R. Fischer, Phys. Rev. Lett. **97**, 200601 (2006).

[48] H. Saito, Y. Kawaguchi, and M. Ueda, Phys. Rev. A **76**, 043613 (2007).

[49] V. Mukherjee, U. Divakaran, A. Dutta, and D. Sen, Phys. Rev. B **76**, 174303 (2007).

[50] F. M. Cucchietti, B. Damski, J. Dziarmaga, and W. H. Zurek, Phys. Rev. A **75**, 023603 (2007).

[51] L. Cincio, J. Dziarmaga, M. M. Rams, and W. H. Zurek, Phys. Rev. A **75**, 052321 (2007).

[52] A. Polkovnikov and V. Gritsev, Nat. Phys. **4**, 477 (2008).

[53] K. Sengupta, D. Sen, and S. Mondal, Phys. Rev. Lett. **100**, 077204 (2008).

[54] J. Dziarmaga, J. Meisner, and W. H. Zurek, Phys. Rev. Lett. **101**, 115701 (2008).

[55] B. Damski and W. H. Zurek, Phys. Rev. Lett. **104**, 160404 (2010).

[56] C. De Grandi, V. Gritsev, and A. Polkovnikov, Phys. Rev. B **81**, 012303 (2010).

[57] F. Pollmann, S. Mukerjee, A. G. Green, and J. E. Moore, Phys. Rev. E **81**, 020101(R) (2010).

[58] B. Damski, H. T. Quan, and W. H. Zurek, Phys. Rev. A **83**, 062104 (2011).

[59] W. H. Zurek, J. Phys.: Condens. Matter **25**, 404209 (2013).

[60] S. Sharma, S. Suzuki, and A. Dutta, Phys. Rev. B **92**, 104306 (2015).

[61] A. Dutta and A. Dutta, Phys. Rev. B **96**, 125113 (2017).

[62] A. Sinha, M. M. Rams, and J. Dziarmaga, Phys. Rev. B **99**, 094203 (2019).

[63] M. M. Rams, J. Dziarmaga, and W. H. Zurek, Phys. Rev. Lett. **123**, 130603 (2019).

[64] S. Mathey and S. Diehl, Phys. Rev. Res. **2**, 013150 (2020).

[65] B. S. Revathy and U. Divakaran, J. Stat. Mech. (2020) 023108.

[66] D. Sen, K. Sengupta, and S. Mondal, Phys. Rev. Lett. **101**, 016806 (2008).

[67] L. E. Sadler, J. M. Higbie, S. R. Leslie, M. Vengalattore, and D. M. Stamper-Kurn, Nature (London) **443**, 312 (2006).

[68] M. Anquez, B. A. Robbins, H. M. Bharath, M. Boguslawski, T. M. Hoang, and M. S. Chapman, Phys. Rev. Lett. **116**, 155301 (2016).

[69] K. Baumann, R. Mottl, F. Brennecke, and T. Esslinger, Phys. Rev. Lett. **107**, 140402 (2011).

[70] L. W. Clark, L. Feng, and C. Chin, Science **354**, 606 (2016).

[71] D. Chen, M. White, C. Borries, and B. DeMarco, Phys. Rev. Lett. **106**, 235304 (2011).

[72] S. Braun, M. Friesdorf, S. S. Hodgman, M. Schreiber, J. P. Ronzheimer, A. Riera, M. del Rey, I. Bloch, J. Eisert, and U. Schneider, Proc. Natl. Acad. Sci. USA **112**, 3641 (2015).

[73] B. Gardas, J. Dziarmaga, W. H. Zurek, and M. Zwolak, Sci. Rep. **8**, 4539 (2018).

[74] C. Meldgin, U. Ray, P. Russ, D. Chen, D. M. Ceperley, and B. DeMarco, Nat. Phys. **12**, 646 (2016).

[75] A. Keesling, A. Omran, H. Levine, H. Bernien, H. Pichler, S. Choi, R. Samajdar, S. Schwartz, P. Silvi, S. Sachdev, P. Zoller, M. Endres, M. Greiner, V. Vuletić, and M. D. Lukin, Nature (London) **568**, 207 (2019).

[76] M. Kolodrubetz, B. K. Clark, and D. A. Huse, Phys. Rev. Lett. **109**, 015701 (2012).

[77] A. Francuz, J. Dziarmaga, B. Gardas, and W. H. Zurek, Phys. Rev. B **93**, 075134 (2016).

[78] A. Chandran, A. Erez, S. S. Gubser, and S. L. Sondhi, Phys. Rev. B **86**, 064304 (2012).

[79] T. W. B. Kibble and G. E. Volovik, JEPT Lett. **65**, 102 (1997).

[80] W. H. Zurek, Phys. Rev. Lett. **102**, 105702 (2009).

[81] A. del Campo, G. De Chiara, G. Morigi, M. B. Plenio, and A. Retzker, Phys. Rev. Lett. **105**, 075701 (2010).

[82] A. del Campo, A. Retzker, and M. B. Plenio, New J. Phys. **13**, 083022 (2011).

[83] A. del Campo, T. W. B. Kibble, and W. H. Zurek, J. Phys.: Condens. Matter **25**, 404210 (2013).

[84] J. Dziarmaga and M. M. Rams, New J. Phys. **12**, 055007 (2010); **12**, 103002 (2010).

[85] M. Collura and D. Karevski, Phys. Rev. Lett. **104**, 200601 (2010); Phys. Rev. A **83**, 023603 (2011).

[86] M. M. Rams, M. Mohseni, and A. del Campo, New J. Phys. **18**, 123034 (2016).

[87] K. Agarwal, R. N. Bhatt, and S. L. Sondhi, Phys. Rev. Lett. **120**, 210604 (2018).

[88] M. Mohseni, J. Strumpfer, and M. M. Rams, New J. Phys. **20**, 105002 (2018).

[89] F. J. Gómez-Ruiz and A. del Campo, Phys. Rev. Lett. **122**, 080604 (2019).

[90] P. Calabrese and J. Cardy, Phys. Rev. Lett. **96**, 136801 (2006).

[91] T. D. Schultz, D. C. Mattis, and E. H. Lieb, Rev. Mod. Phys. **36**, 856 (1964).

[92] P. C. Hohenberg and B. I. Halperin, Rev. Mod. Phys. **49**, 435 (1977).

[93] A. J. Bray, Adv. Phys. **51**, 481 (2002).

[94] R. B. Griffiths, Phys. Rev. Lett. **23**, 17 (1969).

[95] B. M. McCoy, Phys. Rev. B **2**, 2795 (1970).

[96] F. Iglói, R. Juhász, and P. Lajkó, Phys. Rev. Lett. **86**, 1343 (2001).

[97] D. S. Fisher, Phys. Rev. Lett. **69**, 534 (1992).

[98] D. S. Fisher, Phys. Rev. B **51**, 6411 (1995).

[99] B. M. McCoy and T. T. Wu, Phys. Rev. **176**, 631 (1968).

[100] J. Dziarmaga, Phys. Rev. B **74**, 064416 (2006).

[101] T. Caneva, R. Fazio, and G. E. Santoro, Phys. Rev. B **76**, 144427 (2007).

[102] L. Cincio, J. Dziarmaga, J. Meisner, and M. M. Rams, Phys. Rev. B **79**, 094421 (2009).

[103] D. Vodola, L. Lepori, E. Ercolessi, A. V. Gorshkov, and G. Pupillo, Phys. Rev. Lett. **113**, 156402 (2014).

[104] D. Vodola, L. Lepori, E. Ercolessi, and G. Pupillo, New J. Phys. **18**, 015001 (2015).

[105] P. Hauke and L. Tagliacozzo, Phys. Rev. Lett. **111**, 207202 (2013).

[106] J. Eisert, M. van den Worm, S. R. Manmana, and M. Kastner, Phys. Rev. Lett. **111**, 260401 (2013).

[107] L. Cevolani, G. Carleo, and L. Sanchez-Palencia, New J. Phys. **18**, 093002 (2016).

[108] N. Defenu, T. Enss, M. Kastner, and G. Morigi, Phys. Rev. Lett. **121**, 240403 (2018).

[109] D. Sadhukhan and J. Dziarmaga (unpublished).

[110] D. Jaschke, K. Maeda, J. D. Whalen, M. L. Wall, and L. D. Carr, New J. Phys. **19**, 033032 (2017).

[111] N. Defenu, G. Morigi, L. Dell'Anna, and T. Enss, Phys. Rev. B **100**, 184306 (2019).

[112] R. Puebla, O. Marty, and M. B. Plenio, Phys. Rev. A **100**, 032115 (2019).

[113] B. Damski and W. H. Zurek, Phys. Rev. A **73**, 063405 (2006).

[114] A. P. Young, Phys. Rev. B **56**, 11691 (1997).

[115] E. Barouch and B. M. McCoy, Phys. Rev. A **3**, 786 (1971).

[116] N. Defenu, T. Enss, and J. C. Halimeh, Phys. Rev. B **100**, 014434 (2019).

[117] F. W. J. Olver, D. W. Lozier, R. F. Boisvert, and C. W. Clark, *NIST Handbook of Mathematical Functions* (Cambridge University Press, Cambridge, UK, 2010).

[118] M. Abramowitz and I. A. Stegun, *Handbook of Mathematical Functions* (National Bureau of Standards, Washington, D.C., 1970).